

Neural Sheaf Diffusion: A Topological Perspective on Heterophily and Oversmoothing in GNNs

Cristian Bodnar^{† 1} Francesco Di Giovanni^{‡ 2} Benjamin P. Chamberlain² Pietro Liò¹ Michael M. Bronstein^{2,3}

Abstract

Cellular sheaves equip graphs with “geometrical” structure by assigning vector spaces and linear maps to nodes and edges. Graph Neural Networks (GNNs) implicitly assume a graph with a trivial underlying sheaf. This choice is reflected in the structure of the graph Laplacian operator, the properties of the associated diffusion equation, and the characteristics of the convolutional models that discretise this equation. In this paper, we use cellular sheaf theory to show that the underlying geometry of the graph is deeply linked with the performance of GNNs in heterophilic settings and their oversmoothing behaviour. By considering a hierarchy of increasingly general sheaves, we study how the ability of the sheaf diffusion process to achieve linear separation of the classes in the infinite time limit expands. At the same time, we prove that when the sheaf is non-trivial, discretised parametric diffusion processes have greater control than GNNs over their asymptotic behaviour. On the practical side, we study how sheaves can be learned from data. The resulting sheaf diffusion models have many desirable properties that address the limitations of classical graph diffusion equations (and corresponding GNN models) and obtain state-of-the-art results in heterophilic settings. Overall, our work provides new connections between GNNs and algebraic topology and would be of interest to both fields.

1. Introduction

Graph Neural Networks (GNNs) (Sperduti, 1994; Goller & Kuchler, 1996; Gori et al., 2005; Scarselli et al., 2008; Bruna et al., 2014; Defferrard et al., 2016; Kipf & Welling,

[†]Work done as a research intern at Twitter [‡]Proved the results in Section 3 ¹Department of Computer Science, University of Cambridge, Cambridge, UK ²Twitter, UK ³Department of Computer Science, University of Oxford, Oxford, UK. Correspondence to: Cristian Bodnar <cb2015@cam.ac.uk>.

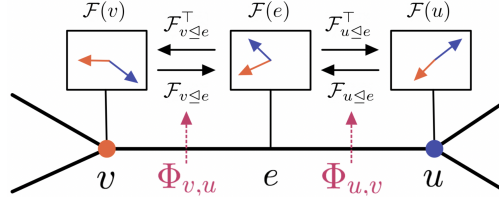


Figure 1. A sheaf (G, \mathcal{F}) illustrated for a single edge of the graph. The stalks $\mathcal{F}(v), \mathcal{F}(u), \mathcal{F}(e)$ are isomorphic to \mathbb{R}^2 . The restriction maps $\mathcal{F}_{v \leq e}, \mathcal{F}_{u \leq e}$ and their adjoints move the vector features between these spaces. In practice, we learn the sheaf from data via a parametric function Φ as indicated by the red dotted lines .

2017; Gilmer et al., 2017) have recently become very popular in the ML community as a model of choice to deal with relational and interaction data due to their multiple successful applications in domains ranging from social science and particle physics to structural biology and drug design.

We focus on two main problems often observed in GNNs: their poor performance in heterophilic graphs (Zhu et al., 2020) and their oversmoothing behaviour (Nt & Maehara, 2019; Oono & Suzuki, 2020). The former arises from the fact that GNNs are usually built on the strong assumption of *homophily*, i.e., that nodes tend to connect to other similar nodes. The latter refers to a phenomenon of deeper GNNs producing features that are too smooth to be useful.

In this work, we show that these two fundamental problems are linked by a common cause: the underlying “geometry” of the graph (used here in a very loose sense). When this geometry is trivial, as is typically the case, the two phenomena described above emerge. We make these statements precise through the lens of cellular sheaf theory (Curry, 2014), a subfield of algebraic topology (Hatcher, 2000). Intuitively, a cellular sheaf associates a vector space to each node and edge of a graph, and a linear map between these spaces for each incident node-edge pair (Figure 1).

In Section 4 we analyse how by considering a hierarchy of increasingly general sheaves, starting from a trivial one, a diffusion equation based on the sheaf Laplacian (Hansen & Ghrist, 2019) can solve increasingly more complicated node-classification tasks in the infinite time limit. In this regime, we show that oversmoothing can be avoided by equipping the graph with the right sheaf structure for a task.

In Section 5, we study the behaviour of a non-linear, parametric, and discrete version of this process. This results in a *Sheaf Convolutional Network* (Hansen & Gebhart, 2020) that generalises GCN of Kipf & Welling (2017). We prove that this discrete diffusion process does not necessarily converge to the harmonic space of the sheaf Laplacian, even when the norm of the weights is controlled from above, in contrast to GCNs (Cai & Wang, 2020; Oono & Suzuki, 2019). In other words, the weights can steer the diffusion process to a larger extent, which is important when the underlying sheaf is only approximately correct.

All these results are based on the properties of the harmonic space of the sheaf Laplacian. We begin by studying these properties from a spectral perspective in Section 3. We provide a new Cheeger-type inequality for the spectral gap of the sheaf Laplacian and note that these results might be of independent interest for spectral sheaf theory.

Finally, in Section 6, we apply our theory for designing simple and practical GNN models. We describe how to construct such models by learning sheaves from data. The resulting sheaf models obtain state-of-the-art results in heterophilic graphs and show strong performance in homophilic ones.

To summarise our contributions: We (1) introduce a novel Graph ML framework based on cellular sheaves; (2) Prove new results about the spectral properties of the sheaf Laplacian that improve our understanding of its harmonic space; (3) Study the linear separation power of sheaf diffusion equations in node classification tasks and demonstrate it can avoid oversmoothing; (4) Prove that a nonlinear sheaf-based GCN-like operator can steer the diffusion process, unlike in the classical case; (5) Show how to learn sheaves from data and construct sheaf diffusion-based GNN models that obtain state-of-the-art results on heterophilic datasets.

2. Background

A *cellular sheaf* (Curry, 2014) over a graph (Figure 1) is a mathematical object associating a space with each node and edge in the graph and a map between these spaces for each incident node-edge pair. We define this formally below:

Definition 1. A *cellular sheaf* (G, \mathcal{F}) on an undirected graph $G = (V, E)$ consists of:

- A vector space $\mathcal{F}(v)$ for each $v \in V$.
- A vector space $\mathcal{F}(e)$ for each $e \in E$.
- A linear map $\mathcal{F}_{v \leq e} : \mathcal{F}(v) \rightarrow \mathcal{F}(e)$ for each incident $v \leq e$ node-edge pair.

The vector spaces of the nodes and edges are called *stalks*, while the linear maps are referred to as *restriction maps*.

The space formed by all the spaces associated to the nodes of the graph is called the space of *0-cochains* and is denoted by $C^0(G, \mathcal{F})$. Similarly, $C^1(G, \mathcal{F})$ – the space of *1-cochains* – contains the data associated with all the edges of the graph.

Definition 2. For a sheaf (\mathcal{F}, G) we define the space of 0-cochains $C^0(G; \mathcal{F}) := \bigoplus_{v \in V} \mathcal{F}(v)$ and 1-cochains $C^1(G; \mathcal{F}) := \bigoplus_{e \in E} \mathcal{F}(e)$.

For a 0-cochain $\mathbf{x} \in C^0(G; \mathcal{F})$, we use \mathbf{x}_v to refer to the vector in $\mathcal{F}(v)$ of node v and similarly for 1-cochains. From an opinion dynamics perspective (Hansen & Ghrist, 2021), \mathbf{x}_v can be thought of as the private opinion of node v , while $\mathcal{F}_{v \leq e}$ expressed how that opinion manifests publicly in a discourse space formed by $\mathcal{F}(e)$. It is natural to define a linear *co-boundary map* δ between $C^0(G, \mathcal{F})$ and $C^1(G, \mathcal{F})$, which measures the disagreement between all nodes in the discourse space.

Definition 3. For some arbitrary choice of orientation for each edge $e = u \rightarrow v \in E$, $\delta : C^0(G, \mathcal{F}) \rightarrow C^1(G, \mathcal{F})$, $\delta(\mathbf{x})_e := \mathcal{F}_{v \leq e} \mathbf{x}_v - \mathcal{F}_{u \leq e} \mathbf{x}_u$.

Given a cellular sheaf (G, \mathcal{F}) , using the co-boundary operator δ , one can define a *Sheaf Laplacian* operator associated with the sheaf (Hansen & Ghrist, 2019).

Definition 4. The *sheaf Laplacian* of a sheaf (G, \mathcal{F}) is a map $L_{\mathcal{F}} : C^0(G, \mathcal{F}) \rightarrow C^0(G, \mathcal{F})$ given by $L_{\mathcal{F}} := \delta^{\top} \delta$.

$$L_{\mathcal{F}}(\mathbf{x})_v := \sum_{v, u \leq e} \mathcal{F}_{v \leq e}^{\top} (\mathcal{F}_{v \leq e} \mathbf{x}_v - \mathcal{F}_{u \leq e} \mathbf{x}_u)$$

The sheaf Laplacian is a positive semi-definite block matrix. The diagonal blocks are $L_{\mathcal{F}vv} = \sum_{v \leq e} \mathcal{F}_{v \leq e}^{\top} \mathcal{F}_{v \leq e}$, while the non-diagonal blocks $L_{\mathcal{F}vu} = -\mathcal{F}_{v \leq e}^{\top} \mathcal{F}_{u \leq e}$. A normalised version of this Laplacian can also be defined. Let D be the block-diagonal of $L_{\mathcal{F}}$. Then the normalised-sheaf Laplacian $\Delta_{\mathcal{F}} := D^{-1/2} L_{\mathcal{F}} D^{-1/2}$.

For simplicity, we assume from now on that all the stalks have dimension d . In that case, the sheaf Laplacian is a $nd \times nd$ real matrix, where n is the number of nodes of G . When the vector spaces are set to \mathbb{R} and the linear maps to id , the underlying sheaf is trivial, $d = 1$ and one recovers the well-known $n \times n$ (normalised) graph Laplacian matrix.

The harmonic space of $L_{\mathcal{F}}$ is characterised by the *global sections* of the sheaf.

Definition 5. The global sections of a sheaf form the set:

$$H^0(G; \mathcal{F}) := \{\mathbf{x} \in C^0(G; \mathcal{F}) \mid \mathcal{F}_{v \leq e} \mathbf{x}_v = \mathcal{F}_{u \leq e} \mathbf{x}_u\}$$

This set corresponds to the signals that agree with the restriction maps globally (i.e. along all edges of the graph). The central theorem of discrete Hodge theory says that the space formed by all these 0-cochains is isomorphic to the kernel of the sheaf Laplacian.

Theorem 6. $H^0(G; \mathcal{F})$ and $\ker(L_{\mathcal{F}})$ are isomorphic.

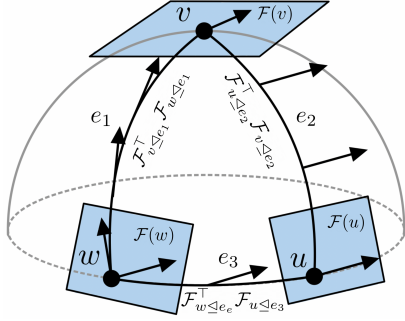


Figure 2. Analogy between parallel transport on a sphere and transport on a discrete vector bundle. A tangent vector is moved from $\mathcal{F}(w) \rightarrow \mathcal{F}(v) \rightarrow \mathcal{F}(u)$ and back. In this particular case, the transport is *not* path-independent because the vector arrives back in a different position from where it started. In the continuous case, this happens because of the curvature of the surface. In the sheaf case, this is purely a consequence of the restriction maps.

The sheaves (G, \mathcal{F}) with orthogonal restriction maps (i.e. $\mathcal{F}_{v \leq e} \in O(d)$ the Lie group of $d \times d$ orthogonal matrices), will play an important role in our analysis. Such sheaves are called *discrete $O(d)$ -bundles* since they can be seen as a discrete equivalent of vector bundles from differential geometry (Tu, 2011). Intuitively, these are objects describing how vector spaces are attached to the points of a manifold. In our case, the role of the manifold is played by the graph.

The sheaf Laplacian of a discrete $O(d)$ -bundle is equivalent to a *connection Laplacian* (Singer & Wu, 2012), describing how the elements of a vector space are transported via rotations in another neighbouring vector space. This is analogous to how tangent vectors are transported across a manifold (see Figure 2).

3. Harmonic Space of Sheaf Laplacians

In this section we study general properties of the harmonic space $\ker(\Delta_{\mathcal{F}})$ of the normalised sheaf Laplacian. As with the normalised graph Laplacian, the normalised sheaf Laplacian is preferred for most practical purposes because its spectrum is bounded. Since a major role in the analysis below is played by discrete vector bundles, we focus on this case. We note though, that our results below generalise to the general linear group $\mathcal{F}_{v \leq e} \in GL(d)$, the Lie group of $d \times d$ invertible matrices, provided we can also control the norm of the restriction maps from below.

Given a discrete $O(d)$ -bundle, the block diagonal of $\mathcal{L}_{\mathcal{F}}$ has a block structure since $\mathcal{L}_{\mathcal{F}vv} = d_v \mathbf{I}_d$, where d_v is the degree of node v . Accordingly, if a signal $\tilde{\mathbf{x}} \in \ker(\mathcal{L}_{\mathcal{F}})$, then the signal $\mathbf{x} : v \mapsto \sqrt{d_v} \mathbf{x}_v \in \ker(\Delta_{\mathcal{F}})$ and similarly for the inverse transformation. In general the harmonic space may be trivial: this happens when the constraints $\mathcal{F}_{v \leq e} \mathbf{x}_v = \mathcal{F}_{u \leq e} \mathbf{x}_u$ are not compatible with each other. Since the harmonic space will be related to the linear sepa-

ration power of sheaf diffusion, we investigate below when this space is non-empty and derive to what extent the graph structure affects that. Key to our analysis is studying *transport* operators induced by the restriction maps of the sheaf.

Given nodes $v, u \in V$ and a path $\gamma_{v \rightarrow u} = (v, v_1, \dots, v_\ell, u)$ from v to u , we consider a notion of **transport** from the stalk $\mathcal{F}(v)$ to the stalk $\mathcal{F}(u)$ via map composition:

$$\mathbf{P}_{v \rightarrow u}^\gamma := (\mathcal{F}_{u \leq e}^\top \mathcal{F}_{v_L \leq e}) \dots (\mathcal{F}_{v_1 \leq e}^\top \mathcal{F}_{v \leq e}) : \mathcal{F}(v) \rightarrow \mathcal{F}(u).$$

In general then, transport maps act on node stalks and are constructed by composing single restriction maps (and their transpose) along edges.

For general sheaf structures, the graph transport is *path dependent*, meaning that how the vectors are transported across two nodes depends on the path between them (see Figure 2). In fact, we show that this property characterises the *spectral gap* of a sheaf Laplacian (we note again that, differently from the classical case, the kernel of $\Delta_{\mathcal{F}}$ may be trivial, so by ‘spectral gap’ we refer here to the value of the smallest eigenvalue of $\Delta_{\mathcal{F}}$).

Proposition 7. *If \mathcal{F} is a discrete $O(d)$ bundle over a connected graph and $r := \max_{\gamma_{v \rightarrow u}, \gamma'_{v \rightarrow u}} \|\mathbf{P}_{v \rightarrow u}^\gamma - \mathbf{P}_{v \rightarrow u}^{\gamma'}\|$, then we have $\lambda_0^{\mathcal{F}} \leq \frac{r^2}{2}$.*

A consequence of the previous result is that there is always a non-trivial harmonic space (i.e. $\lambda_0^{\mathcal{F}} = 0$) if the transport maps generated by an orthogonal sheaf are *path-independent*. Next, we address the opposite direction.

Proposition 8. *If \mathcal{F} is a discrete $O(d)$ bundle over a connected graph and $\mathbf{x} \in H^0(G, \mathcal{F})$, then for any cycle γ based at $v \in V$ we have $\mathbf{x}_v \in \ker(\mathbf{P}_{v \rightarrow v}^\gamma - \mathbf{I})$.*

The previous proposition highlights the interplay between the graph and the sheaf structure. In fact, a simple consequence of this result is that for any cycle-free subset $S \subset V$, we have that any connection Laplacian restricted to S always admits a non-trivial harmonic space.

A natural question connected to the previous result is whether a Cheeger-like inequality holds in the other direction. This turns out to be the case.

Proposition 9. *Let \mathcal{F} be a discrete $O(d)$ bundle over a connected graph G with n nodes and let $\|\mathbf{P}_{v \rightarrow v}^\gamma - \mathbf{I}\| \geq \epsilon \|\mathbf{x}\|$ for all cycles $\gamma_{v \rightarrow v}$. Then $\lambda_0^{\mathcal{F}} \geq \epsilon^2 (2\text{diam}(G)n d_{\max})^{-1}$.*

While the bound above is of little use in practice, it shows how the spectral gap of a sheaf Laplacian is indeed related to the deviation of the transport maps from being path-independent. We note that the Cheeger-like inequality presented here is not unique and other types of bounds on $\lambda_0^{\mathcal{F}}$ have been derived by Bandeira et al. (2013).

We conclude this section by further analysing the dimensionality of the harmonic space of discrete $O(d)$ -bundles.

Lemma 10. *Let \mathcal{F} be a discrete $O(d)$ bundle over a connected graph G . Then $\dim(H^0) \leq d$ and $\dim(H^0) = d$ iff the transport is path-independent.*

4. The Separation Power of Sheaf Diffusion

Preliminaries Let $G = (V, E)$ be a graph and consider that all nodes have features that are d -dim vectors $\mathbf{x}_v \in \mathcal{F}(v)$. The features of all nodes are represented as a single vector $\mathbf{x} \in C^0(G; \mathcal{F})$ stacking all the individual d -dim vectors. Additionally, if we allow for f feature channels, everything can be represented as a matrix $\mathbf{X} \in \mathbb{R}^{(nd) \times f}$, whose columns are vectors in $C^0(G; \mathcal{F})$.

In this section, we are interested in the spatially discretised *sheaf diffusion* process governed by the PDE:

$$\mathbf{X}(0) = \mathbf{X}, \quad \dot{\mathbf{X}}(t) = -\Delta_{\mathcal{F}} \mathbf{X}(t) \quad (1)$$

It can be shown that in the time limit, each feature channel is projected into the harmonic space of the sheaf Laplacian $\ker(\Delta_{\mathcal{F}})$ (Hansen & Ghrist, 2019). Up to a $D^{-1/2}$ normalisation, this space contains the signals that agree with the restriction maps of the sheaf along all the edges. Thus, sheaf diffusion can be seen as a global ‘synchronisation’ process.

We now analyse the ability of certain classes of sheaf Laplacian operators to linearly separate the features in the limit of the diffusion processes they induce. We consider this a proxy for the capacity of certain diffusion processes to avoid oversmoothing.

Definition 11. *A hypothesis class of sheaves with d -dimensional stalks \mathcal{H}^d has linear separation power over a set of graphs \mathcal{G} iff for any labelled graph $G = (V, E) \in \mathcal{G}$, there is a sheaf $(\mathcal{F}, G) \in \mathcal{H}^d$ that can linearly separate the classes of G in the time limit of Equation 1 for a dense subset $\mathcal{X}_{\mathcal{F}} \subset \mathbb{R}^{nd \times f}$ of initial conditions.*

The restriction to a set of initial conditions that is dense in the ambient space is necessary because, in the limit, diffusion behaves like a projection in the harmonic space and there will always be degenerate initial conditions that will yield a zero projection.

Definition 12. *Consider the class of sheaves with symmetric and invertible transport maps and d -dimensional stalks.*

$$\mathcal{H}_{\text{sym}}^d := \{(\mathcal{F}, G) \mid \mathcal{F}_{v \leq e} = \mathcal{F}_{u \leq e}, \det(\mathcal{F}_{v \leq e}) \neq 0\}$$

We note that for $d = 1$, the sheaf Laplacians induced by this class of sheaves coincides with the set of the well-known weighted graph Laplacians with strictly positive weights, which also includes the usual graph Laplacian (see proof in Appendix B). Therefore, this hypothesis class is of particular

interest since it includes those graph Laplacians typically used by graph convolutional models such as GCN (Kipf & Welling, 2017) and ChebNet (Defferrard et al., 2016).

We first show that this class of sheaf Laplacians can linearly separate the classes in binary classification settings under certain homophily assumptions:

Proposition 13. *Let \mathcal{G} be the set of connected graphs $G = (V, E)$ with two classes $A, B \subset V$ such that for each $v \in A$, there exists $u \in A$ and an edge $(v, u) \in E$. Then $\mathcal{H}_{\text{sym}}^1$ has linear separation power over \mathcal{G} .*

In contrast, under certain heterophilic conditions, this hypothesis class is not powerful enough to linearly separate the two classes no matter what the initial conditions are:

Proposition 14. *Let \mathcal{G} be the set of connected bipartite graphs $G = (A, B, E)$, with partitions A, B forming two classes and $|A| = |B|$. Then $\mathcal{H}_{\text{sym}}^1$ cannot linearly separate any graph in \mathcal{G} for any initial conditions $\mathbf{X}(0) \in \mathbb{R}^{n \times f}$.*

We now consider a larger hypothesis class that also includes non-symmetric relations.

Definition 15. *The the class of sheaves with invertible maps and d -dimensional stalks:*

$$\mathcal{H}^d := \{(\mathcal{F}, G) \mid \det(\mathcal{F}_{v \leq e}) \neq 0\}$$

Proposition 16. *Let \mathcal{G} contain all the connected graphs with two classes. Then, \mathcal{H}^1 has linear separation power over \mathcal{G} .*

These results show that heterophilic settings require an asymmetric transport of the features between neighbouring nodes belonging to different classes. This provides a sheaf-theoretic explanation for why a recent body of work (Yan et al., 2021; Chien et al., 2021; Bo et al., 2021) has found negatively-weighted edges to help in heterophilic settings. From this perspective, negatively-signed edges constrain the product $\mathcal{F}_{v \leq e} \mathcal{F}_{u \leq e}$ of an implicit underlying sheaf to be negative and hence $\mathcal{F}_{v \leq e} \neq \mathcal{F}_{u \leq e}$. As the next result shows, in $d = 1$, signed relations are a particularly important way to achieve this asymmetry:

Definition 17. *The class of sheaves over G with non-zero maps, one-dimensional stalks, and similarly signed restriction maps:*

$$\mathcal{H}_+^1 := \{(\mathcal{F}, G) \mid \mathcal{F}_{v \leq e} \mathcal{F}_{u \leq e} > 0\}$$

Proposition 18. *Let G be the connected graph with two nodes belonging to two different classes. Then \mathcal{H}_+^1 cannot linearly separate the two nodes for any initial conditions $\mathbf{X} \in \mathbb{R}^{2 \times f}$.*

This shows that even the simplest heterophilic graph still cannot be distinguished in this case even with asymmetric transport maps unless $\mathcal{F}_{v \leq e}, \mathcal{F}_{u \leq e}$ have opposite signs.

So far we have only studied the effects of changing the type of sheaves in dimension one. We now consider the effects of adjusting the dimension of the stalks and begin by stating a fundamental limitation of (sheaf) diffusion when $d = 1$.

Proposition 19. *Let G be a connected graph with $C \geq 3$ classes. Then \mathcal{H}^1 cannot linearly separate any $\mathbf{X} \in \mathbb{R}^{n \times f}$.*

This is essentially a consequence of $\dim(\ker(\Delta_{\mathcal{F}}))$ being at most one in this case, as described by Lemma 10. From a GNN perspective, this means that in the infinite depth setting, sufficient *stalk width* (i.e., dimension) is needed in order to solve tasks involving more than two classes. Note that this notion of width given by d is different from the classical notion given by the number of feature channels f . As the result above shows, the latter has no effect on the linear separability of the classes. Next, we will see that the former does.

Definition 20. *Consider the class of sheaves with diagonal invertible maps and d -dimensional stalks:*

$$\mathcal{H}_{\text{diag}}^d := \{(\mathcal{F}, G) \mid \mathcal{F}_{v \leq e} = \text{invertible diagonal matrix}\}$$

Proposition 21. *Let \mathcal{G} be the set of connected graphs with nodes belonging to $C \geq 3$ classes. Then for $d \geq C$, $\mathcal{H}_{\text{diag}}^d$ has linear separation power over \mathcal{G} .*

This proposition illustrates the benefits of using higher-dimensional stalks, while maintaining a simple and computationally convenient class of diagonal restriction maps.

By using more complex restriction maps, we can show that lower-dimensional stalks can be used to achieve linear separation in the presence of even more classes.

Definition 22. *The class of discrete $O(d)$ -bundles:*

$$\mathcal{H}_{\text{orth}}^d := \{(\mathcal{F}, G) \mid \mathcal{F}_{v \leq e} \in O(d)\}$$

We show that for stalks of dimension $d \in \{2, 4\}$, one can classify at least $C = 2d$ classes.

Theorem 23. *Let \mathcal{G} be the class of connected graphs with $C \leq 2d$ classes. Then, for all $d \in \{2, 4\}$, $\mathcal{H}_{\text{orth}}^d$ has linear separation power over \mathcal{G} .*

This shows that orthogonal maps are able to make more efficient use of the space available to them than diagonal restriction maps. Our proof relies on the algebra of quaternions and their generalisations and also shows the result cannot be extended to other dimensions. We note that with the additional assumption that the graph is regular, this hypothesis class can distinguish an arbitrary number of classes (see Appendix B).

We conclude this section by highlighting that the limitations of symmetric relations persist even in higher dimensions and that Proposition 14 also extends to $\mathcal{H}_{\text{orth,sym}}^d$, the class of $O(d)$ -bundles where for all $v, u \leq e$, $\mathcal{F}_{v \leq e} = \mathcal{F}_{u \leq e}$.

In summary, we showed that: (1) Sheaf diffusion on a trivial sheaf with symmetric (scalar) restriction maps (as implicitly used in standard graph convolutions) has linear separation power only in certain (homophilic) settings. (2) Dealing with heterophilic data and over-smoothing requires non-symmetric restriction maps. (3) Higher-dimensional stalks and more complex restriction maps lead to stronger separation power.

5. Asymptotics of Sheaf Convolutions

In Section 4 we analysed the ability of sheaf diffusion to linearly separate the node-classes in the limit. However, when considering a discrete, parametric and non-linear version of this process, it is important to know how much the weights can steer it. This is particularly relevant if the underlying sheaf is only approximately correct for the task to be solved.

The continuous diffusion process from Equation 1 has the following Euler discretisation with unit step-size:

$$\mathbf{X}(t+1) = \mathbf{X}(t) - \Delta_{\mathcal{F}} \mathbf{X}(t) = (\mathbf{I}_{nd} - \Delta_{\mathcal{F}}) \mathbf{X}(t) \quad (2)$$

Assuming $\mathbf{X} \in \mathbb{R}^{nd \times f_1}$, we can equip the right side with weight matrices $\mathbf{W}_1 \in \mathbb{R}^{d \times d}$, $\mathbf{W}_2 \in \mathbb{R}^{f_1 \times f_2}$ and a non-linearity σ to arrive at the following model originally proposed by Hansen & Gebhart (2020):

$$\mathbf{Y} = \sigma \left((\mathbf{I}_{nd} - \Delta_{\mathcal{F}}) (\mathbf{I}_n \otimes \mathbf{W}_1) \mathbf{X} \mathbf{W}_2 \right) \in \mathbb{R}^{nd \times f_2}, \quad (3)$$

where f_1, f_2 are the number of input and output feature channels, and \otimes denotes the Kronecker product. Here, \mathbf{W}_1 multiplies from the left the vector feature of all the nodes in all channels (i.e. $\mathbf{W}_1 \mathbf{x}_v^i$ for all v and channels i), while \mathbf{W}_2 multiplies the features from the right and can adjust the number of feature channels, just like in GCNs.

It is natural to call this model a **Sheaf Convolutional Network** (SCN) since when $\Delta_{\mathcal{F}}$ is the usual normalised graph Laplacian, \mathbf{W}_1 becomes a scalar and one recovers GCN of Kipf & Welling (2017). To study this prototypical nonlinear and parametric discrete diffusion model in the limit of an infinite number of layers, we adapt the proof technique of Cai & Wang (2020) to track the *sheaf Dirichlet energy* as the signal is passed through multiple SCN layers.

Definition 24. *The sheaf Dirichlet energy $E_{\mathcal{F}}(\mathbf{x})$ of a signal $\mathbf{x} \in C^0(G, \mathcal{F})$ is defined as:*

$$\mathbf{x}^\top \Delta_{\mathcal{F}} \mathbf{x} = \frac{1}{2} \sum_{e:=(v,u)} \|\mathcal{F}_{v \leq e} D_v^{-1/2} \mathbf{x}_v - \mathcal{F}_{u \leq e} D_u^{-1/2} \mathbf{x}_u\|_2^2$$

Similarly, for multiple channels the energy is $\text{trace}(\mathbf{X}^\top \Delta_{\mathcal{F}} \mathbf{X})$. It is easy to see that $\mathbf{x} \in \ker(\Delta_{\mathcal{F}}) \Leftrightarrow E_{\mathcal{F}}(\mathbf{x}) = 0$. Therefore, we can use the energy of a signal as a metric to measure its distance from the harmonic space.

We begin by studying the sheaves for which the features end up asymptotically in $\ker(\Delta_{\mathcal{F}})$. The first such example is for $O(d)$ -bundles with symmetric relations. Let $\lambda_* = \max((\lambda_{\min} - 1)^2, (\lambda_{\max} - 1)^2)$, where $\lambda_{\min}, \lambda_{\max}$ are the smallest and largest non-zero eigenvalues of $\Delta_{\mathcal{F}}$.

Theorem 25. *Let (\mathcal{F}, G) be an $O(d)$ -bundle in $\mathcal{H}_{\text{orth,sym}}^d$ and assume $\sigma = \text{ReLU}$ or LeakyReLU . Then $E_{\mathcal{F}}(\mathbf{Y}) \leq \lambda_* \|\mathbf{W}_1\|_2^2 \|\mathbf{W}_2^\top\|_2^2 E_{\mathcal{F}}(\mathbf{X})$.*

In particular, this means that if $\lambda_* \|\mathbf{W}_1\|_2^2 \|\mathbf{W}_2^\top\|_2^2 < 1$, the signal converges exponentially fast to $\ker(\Delta_{\mathcal{F}})$. In some sense, this is not surprising because when we have symmetric relations along all edges (i.e. $\mathcal{F}_{v \leq e} = \mathcal{F}_{u \leq e}$) and hence the conditions in Theorem 25 are satisfied, then the harmonic space $\ker(\Delta_{\mathcal{F}})$ contain the same information as the kernel of the classical normalised Laplacian Δ_0 .

Proposition 26. *If \mathcal{F} is an $O(d)$ -bundle in $\mathcal{H}_{\text{orth,sym}}^d$, then $\mathbf{x} \in \ker \Delta_{\mathcal{F}}$ if and only if $\mathbf{x}^k \in \ker \Delta_0$ for all $1 \leq k \leq d$.*

Importantly, the symmetry of the relations along all edges is a necessary condition in Theorem 25. As soon as we have an asymmetric transport map, we can find an arbitrarily small linear transformation \mathbf{W} that increases the energy.

Proposition 27. *For any connected graph G and $\varepsilon > 0$, there exist a sheaf (G, \mathcal{F}) , \mathbf{W} with $\|\mathbf{W}\|_2 < \varepsilon$ and feature vector \mathbf{x} such that $E_{\mathcal{F}}((\mathbf{I} \otimes \mathbf{W})\mathbf{x}) > E_{\mathcal{F}}(\mathbf{x})$.*

Beyond $O(d)$ -bundles, we also have the following result for general sheaves with stalks of dimension $d = 1$ which generalises that of [Cai & Wang \(2020\)](#); [Oono & Suzuki \(2019\)](#) for GCNs:

Theorem 28. *Let (\mathcal{F}, G) be a sheaf in \mathcal{H}_+^1 and assume σ is ReLU or LeakyReLU. Then $E_{\mathcal{F}}(\mathbf{Y}) \leq \lambda_* \|\mathbf{W}_1\|_2^2 \|\mathbf{W}_2^\top\|_2^2 E_{\mathcal{F}}(\mathbf{X})$.*

As before, having positively-signed relations is a necessary condition in the non-linear case to ensure oversmoothing happens. However, in this case, the proof also holds for negatively-signed relations when using a linear model (i.e. when σ is the identity). Due to this result, we note that [Propositons 14](#) and [19](#) also generalise to GCNs. Any GCN using a weighted graph Laplacian that oversmooths as in Theorem 28 cannot linearly separate more than two classes. Furthermore, such a GCN cannot separate the classes of a bipartite graph with equally-sized partitions.

We have two main takeaways: (1) Discrete sheaf diffusion models can avoid (in general) the kernel of the diffusion operator even in the deep linear case. (2) The asymmetry of the transport maps play (again) an important role in that.

6. Sheaf Learning

In the previous sections we discussed the various advantages one obtains from using the right sheaf-structure for a particular node classification task. However, in general, this ground truth sheaf is unknown or unspecified. Therefore, we aim to learn the underlying sheaf from data.

6.1. Sheaf-based GNN Model

We consider the following diffusion-type equation, which contains the sheaf diffusion equation as a particular case.

$$\dot{\mathbf{X}}(t) = -\sigma(\Delta_{\mathcal{F}(t)}(\mathbf{I}_n \otimes \mathbf{W}_1)\mathbf{X}(t)\mathbf{W}_2), \quad (4)$$

Crucially, the sheaf Laplacian $\Delta_{\mathcal{F}(t)}$ is that of a sheaf $(G, \mathcal{F}(t))$ that *evolves over time*. More specifically, the evolution of the sheaf structure is described by a learnable function of the data $(G, \mathcal{F}(t)) = g(G, \mathbf{X}(t); \theta)$.

We also consider a discrete version of this equation, using a new set of weights at each layer t .

$$\mathbf{X}_{t+1} = \mathbf{X}_t - \sigma(\Delta_{\mathcal{F}(t)}(\mathbf{I} \otimes \mathbf{W}_1^t)\mathbf{X}_t\mathbf{W}_2^t), \quad (5)$$

For both, models we use an initial MLP to compute $\mathbf{X}(0)$ from the raw features and a final linear layer to perform the node classification.

Overall, this represents an entirely new framework for learning on graphs, which does not only evolve the features at each new layer, but also evolves the underlying ‘geometry’ of the graph (i.e., the sheaf structure).

6.2. Learning the restriction maps

The advantage of learning a sheaf is that one does not require any sort of embedding of the nodes in an ambient space (as e.g. done in [\(Chamberlain et al., 2021a\)](#)). Instead, everything can be learned *locally*. Each $d \times d$ matrix $\mathcal{F}_{v \leq e}$ is learned via a parametric function $\Phi : \mathbb{R}^{d \times 2} \rightarrow \mathbb{R}^{d \times d}$:

$$\mathcal{F}_{v \leq e:=(v,u)} = \Phi(\mathbf{x}_v, \mathbf{x}_u) \quad (6)$$

For simplicity, the equation above uses a single feature channel, but in practice, all channels are supplied as input. This function retains the inductive bias of locality specific to GNNs since it only utilises the features of the nodes forming the edge. At the same time, it is important that this function is non-symmetric in order to be able learn asymmetric transport maps along each edge. In what follows, we distinguish between several types of functions Φ depending on the type of matrix they learn.

Diagonal The main advantage of this parametrization is that fewer parameters need to be learned per edge and the

sheaf Laplacian ends up being a matrix with diagonal blocks, which also results in fewer operations in sparse matrix multiplications. The main disadvantage is that the d dimensions of the stalks do not interact.

Orthogonal In this case, the model effectively learns a discrete vector bundle. Orthogonal matrices provide several advantages: (1) they are able to mix the various dimension of the stalks, (2) the orthogonality constraint prevents overfitting while reducing the number of parameters, (3) they have better understood theoretical properties, and (4) the resulting Laplacians are easier to normalise numerically since the diagonal entries correspond to the degrees of the nodes. In our model, we build orthogonal matrices from a composition of Householder reflections (Mhammedi et al., 2017).

General Finally, we consider the most general option of learning arbitrary matrices. The maximal flexibility provided by these maps can be useful, but it also comes with the danger of overfitting. At the same time, the sheaf Laplacian is more challenging to normalise numerically since one has to compute $D^{-1/2}$ for a positive semi-definite matrix D . To perform this at scale, one has to rely on SVD, whose gradients can be infinite if D has repeated eigenvalues. Therefore, this model is more challenging to train.

Computational Complexity Treating the number of channels and layers as constant, a typical message passing GNN scales with $\mathcal{O}(n + m)$, where n is the number of nodes and m is the number of edges. A sheaf diffusion model with diagonal maps has complexity $\mathcal{O}(d(n + m))$ because the matrix multiplication required to compute the transport maps reduces to a scalar multiplication. When learning orthogonal or general $d \times d$ matrices, the complexity becomes $\mathcal{O}(d^3(n + m))$ because matrix multiplication is $\mathcal{O}(d^3)$. We note that additional costs for the latter methods such as that of SVD for computing $D^{-1/2}$ for general matrices and that of parametrising the orthogonal group can be done in $O(d^3)$, so the overall complexity is not affected.

In practice, we use $1 \leq d \leq 5$ and all the operations above benefit from batched GPU computations in PyTorch (Paszke et al., 2019) which effectively results in a constant overhead. For learning orthogonal matrices, we rely on the library Torch Householder (Obukhov, 2021) which provides support for fast transformations with very large batch sizes.

7. Experiments

Synthetic experiments We first consider a simple synthetic setup given by a connected bipartite graph, where the two partitions form two equally sized classes. We sample the features from two overlapping isotropic Gaussian distri-

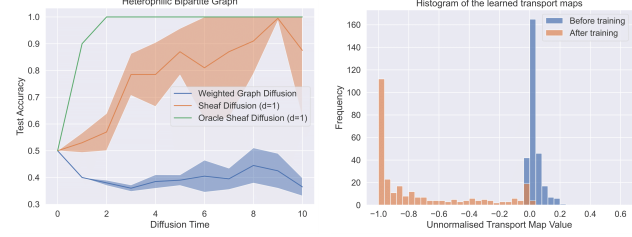


Figure 3. (Left) Test accuracy as a function of diffusion time. (Right) Histogram of the learned scalar transport maps. The performance of the sheaf diffusion model is superior to that of weighted-graph diffusion. The model correctly learns to invert the features of the two classes via the transport maps.

butions in order to make the classes linearly non-separable at initialisation time. From Proposition 14 we know that diffusion models using symmetric restriction maps cannot separate the classes in the limit, while a diffusion process using asymmetric maps should be able to.

Therefore, we consider two simple versions of the model from Equation 4, where we set $\mathbf{W}_1 = \mathbf{I}_d$, $\mathbf{W}_2 = \mathbf{I}_f$ and $\sigma = \text{id}$. In the first, the maps $\mathcal{F}_{v \leq e = (v, u)}$ are learned by a simple layer of the form $\sigma(\mathbf{w}^\top [\mathbf{x}_v || \mathbf{x}_u])$, where $\sigma = \tanh$. For the second model, we use a similar layer but constraint $\mathcal{F}_{v \leq e} = \mathcal{F}_{u \leq e} > 0$, which results in a weighted graph Laplacian.

Figure 3 presents the results of this experiment across five seeds. As expected, for diffusion time zero (i.e. no diffusion), we see that a linear classifier cannot separate the classes. Also as expected, the diffusion process using symmetric maps cannot perfectly fit the data. In contrast, with the more general sheaf diffusion, as more diffusion is performed and the signal approaches the harmonic space, the model gets better and the features become linearly separable. In the second subfigure we take a closer look at the sheaf that the model learns in the time limit by plotting a histogram of all the transport (scalar) maps $\mathcal{F}_{v \leq e}^\top \mathcal{F}_{u \leq e}$. In accordance with Propositions 16 and 18, the model learns a negative transport map for all edges. We discuss this in more detail together with additional synthetic experiments in higher-dimensions in Appendix E.

Real-world experiments We test our models on real-world datasets proposed by Rozemberczki et al. (2021); Pei et al. (2020) to evaluate heterophilic learning. These datasets have an edge homophily coefficient h ranging from $h = 0.11$ (very heterophilic) to $h = 0.81$ (very homophilic) and therefore offer a view of how a model performs in both regimes. We evaluate our models on the 10 fixed splits provided by Pei et al. (2020) and report the mean accuracy and standard deviation. Each split contains 48%/32%/20% of nodes per class for training, validation and testing, respectively.

	Texas	Wisconsin	Film	Squirrel	Chameleon	Cornell	Citeseer	Pubmed	Cora
Hom level	0.11	0.21	0.22	0.22	0.23	0.30	0.74	0.80	0.81
#Nodes	183	251	7,600	5,201	2,277	183	3,327	18,717	2,708
#Edges	295	466	26,752	198,493	31,421	280	4,676	44,327	5,278
#Classes	5	5	5	5	5	5	7	3	6
Diag-SD	85.67 \pm 6.95	88.63 \pm 2.75	37.79 \pm 1.01	54.78 \pm 1.81	68.68 \pm 1.73	86.49 \pm 7.35	77.14 \pm 1.85	89.42 \pm 0.43	87.14 \pm 1.06
O(d)-SD	85.95 \pm 5.51	89.41 \pm 4.74	37.81 \pm 1.15	56.34 \pm 1.32	68.04 \pm 1.58	84.86 \pm 4.71	76.70 \pm 1.57	89.49 \pm 0.40	86.90 \pm 1.13
Gen-SD	82.97 \pm 5.13	89.21 \pm 3.84	37.80 \pm 1.22	53.17 \pm 1.31	67.93 \pm 1.58	85.68 \pm 6.51	76.32 \pm 1.65	89.33 \pm 0.35	87.30 \pm 1.15
GGCN	84.86 \pm 4.55	86.86 \pm 3.29	37.54 \pm 1.56	55.17 \pm 1.58	71.14 \pm 1.84	85.68 \pm 6.63	77.14 \pm 1.45	89.15 \pm 0.37	87.95 \pm 1.05
H2GCN	84.86 \pm 7.23	87.65 \pm 4.98	35.70 \pm 1.00	36.48 \pm 1.86	60.11 \pm 2.15	82.70 \pm 5.28	77.11 \pm 1.57	89.49 \pm 0.38	87.87 \pm 1.20
GPRGNN	78.38 \pm 4.36	82.94 \pm 4.21	34.63 \pm 1.22	31.61 \pm 1.24	46.58 \pm 1.71	80.27 \pm 8.11	77.13 \pm 1.67	87.54 \pm 0.38	87.95 \pm 1.18
FAGCN	82.43 \pm 6.89	82.94 \pm 7.95	34.87 \pm 1.25	42.59 \pm 0.79	55.22 \pm 3.19	79.19 \pm 9.79	N/A	N/A	N/A
MixHop	77.84 \pm 7.73	75.88 \pm 4.90	32.22 \pm 2.34	43.80 \pm 1.48	60.50 \pm 2.53	73.51 \pm 6.34	76.26 \pm 1.33	85.31 \pm 0.61	87.61 \pm 0.85
GCNII	77.57 \pm 3.83	80.39 \pm 3.40	37.44 \pm 1.30	38.47 \pm 1.58	63.86 \pm 3.04	77.86 \pm 3.79	77.33 \pm 1.48	90.15 \pm 0.43	88.37 \pm 1.25
Geom-GCN	66.76 \pm 2.72	64.51 \pm 3.66	31.59 \pm 1.15	38.15 \pm 0.92	60.00 \pm 2.81	60.54 \pm 3.67	78.02 \pm 1.15	89.95 \pm 0.47	85.35 \pm 1.57
PairNorm	60.27 \pm 4.34	48.43 \pm 6.14	27.40 \pm 1.24	50.44 \pm 2.04	62.74 \pm 2.82	58.92 \pm 3.15	73.59 \pm 1.47	87.53 \pm 0.44	85.79 \pm 1.01
GraphSAGE	82.43 \pm 6.14	81.18 \pm 5.56	34.23 \pm 0.99	41.61 \pm 1.74	58.73 \pm 1.68	75.95 \pm 5.01	76.04 \pm 1.30	88.45 \pm 0.50	86.90 \pm 1.04
GCN	55.14 \pm 5.16	51.76 \pm 3.06	27.32 \pm 1.10	53.43 \pm 2.01	64.82 \pm 2.24	60.54 \pm 5.30	76.50 \pm 1.36	88.42 \pm 0.50	86.98 \pm 1.27
GAT	52.16 \pm 6.63	49.41 \pm 4.09	27.44 \pm 0.89	40.72 \pm 1.55	60.26 \pm 2.50	61.89 \pm 5.05	76.55 \pm 1.23	87.30 \pm 1.10	86.33 \pm 0.48
MLP	80.81 \pm 4.75	85.29 \pm 3.31	36.53 \pm 0.70	28.77 \pm 1.56	46.21 \pm 2.99	81.89 \pm 6.40	74.02 \pm 1.90	75.69 \pm 2.00	87.16 \pm 0.37
Cont Diag-SD	82.97 \pm 4.37	86.47 \pm 2.55	36.85 \pm 1.21	38.17 \pm 9.29	62.06 \pm 3.84	80.00 \pm 6.07	76.56 \pm 1.19	89.47 \pm 0.42	86.88 \pm 1.21
Cont O(d)-SD	82.43 \pm 5.95	84.50 \pm 4.34	36.39 \pm 1.37	40.40 \pm 2.01	63.18 \pm 1.69	72.16 \pm 10.40	75.19 \pm 1.67	89.12 \pm 0.30	86.70 \pm 1.24
Cont Gen-SD	83.78 \pm 6.62	85.29 \pm 3.31	37.28 \pm 0.74	52.57 \pm 2.76	66.40 \pm 2.28	84.60 \pm 4.69	77.54 \pm 1.72	89.67 \pm 0.40	87.45 \pm 0.99
BLEND	83.24 \pm 4.65	84.12 \pm 3.56	35.63 \pm 0.89	43.06 \pm 1.39	60.11 \pm 2.09	85.95 \pm 6.82	76.63 \pm 1.60	89.24 \pm 0.42	88.09 \pm 1.22
GRAND	75.68 \pm 7.25	79.41 \pm 3.64	35.62 \pm 1.01	40.05 \pm 1.50	54.67 \pm 2.54	82.16 \pm 7.09	76.46 \pm 1.77	89.02 \pm 0.51	87.36 \pm 0.96
CGNN	71.35 \pm 4.05	74.31 \pm 7.26	35.95 \pm 0.86	29.24 \pm 1.09	46.89 \pm 1.66	66.22 \pm 7.69	76.91 \pm 1.81	87.70 \pm 0.49	87.10 \pm 1.35

Table 1. Results on node classification datasets sorted by their homophily level. The first section includes discrete GNN models, while the second section includes continuous models. Top three models are coloured by **First**, **Second**, **Third**. Our models are marked **-SD**.

Baselines As baselines, we use an ample set of GNN models that can be placed in four categories: (1) classical: GCN (Kipf & Welling, 2017), GAT (Veličković et al., 2018), GraphSAGE (Hamilton et al., 2017); (2) models specifically designed for heterophilic settings: GGCN (Yan et al., 2021), Geom-GCN (Pei et al., 2020), H2GCN (Zhu et al., 2020), GPRGNN (Chien et al., 2021), FAGCN (Bo et al., 2021), MixHop (Abu-El-Haija et al., 2019); (3) models addressing oversmoothing: GCNII (Chen et al., 2020), PairNorm (Zhao & Akoglu, 2020); (4) continuous models: CGNNs (Xhonneux et al., 2020), GRAND (Chamberlain et al., 2021b), and BLEND (Chamberlain et al., 2021a). For (4) we fine-tune and evaluate the models ourselves. The other results are taken from Yan et al. (2021), except for FAGCN and MixHop, which come from Lingam et al. (2021) and Zhu et al. (2020), respectively. All of these were evaluated on the same set of splits as ours.

Results From the results in Table 1 we see that the discrete version of our models are first in 5/6 benchmarks with high heterophily ($h < 0.3$) and second-ranked in the other 1/6. At the same time, the models exhibit strong performance on the homophilic graphs (Cora, Pubmed, Citeseer) being within approximately 1% of the top-performing model. The second part of Table 1 includes continuous models, which our model outperforms on 7/9 benchmarks with particularly large improvements on Chameleon and Squirrel. Among the discrete diffusion models, the $O(d)$ -vector bundle diffusion model performs best overall confirming the intuition that it can better avoid overfitting, while also transforming the vectors in sufficiently complex ways. We also remark the strong performance of the model learning diagonals maps.

8. Discussion and Conclusion

Sheaf Neural Networks Sheaf Neural Networks with a *fixed* sheaf Laplacian were originally introduced by Hansen & Gebhart (2020) in a toy experimental setting. Since then, they have remained completely unexplored. We hope that this paper will fill this lacuna. In contrast to their work, we provide an ample theoretical analysis justifying the use of sheaves in Graph ML. On the practical side, we study for the first time how sheaves can be *learned from data* using neural networks. Finally, this is the first successful application of sheaf-based neural networks in a real-world setting.

Limitations One of the main limitations of our theoretical analysis is that it does not discuss the learnability and generalisation properties of sheaves, only their existence. Nonetheless, this setting was sufficient to produce many valuable insights about heterophily and oversmoothing and a basic understanding of what various types of sheaves can do. Much more theoretical work remains to be done in this direction, and we expect to see further cross-fertilization between ML and algebraic topology research in the future.

Conclusion In this work, we used cellular sheaf theory to provide a novel topological perspective on heterophily and oversmoothing in GNNs. We showed that the underlying sheaf structure of the graph is intimately connected with both of these important factors affecting the performance of GNNs. To mitigate this, we proposed a new paradigm for graph representation learning where models do not only evolve the features at each layer but also the underlying geometry of the graph. In practice, we demonstrated that this framework can achieve state-of-the-art results in heterophilic settings.

Acknowledgements

We are grateful to Iulia Duta, Dobrik Georgiev and Jacob Deasy for valuable comments on an earlier version of this manuscript. CB would also like to thank the Twitter Cortex team for making the research internship a fantastic experience. This research was supported in part by ERC Consolidator grant No. 724228 (LEMAN).

References

Abu-El-Haija, S., Perozzi, B., Kapoor, A., Harutyunyan, H., Alipourfard, N., Lerman, K., Steeg, G. V., and Galstyan, A. Mixhop: Higher-order graph convolutional architectures via sparsified neighborhood mixing. In *The Thirty-sixth International Conference on Machine Learning (ICML)*, 2019. URL <http://proceedings.mlr.press/v97/abu-el-haija19a/abu-el-haija19a.pdf>.

Bandeira, A. S., Singer, A., and Spielman, D. A. A Cheeger inequality for the graph connection laplacian. *SIAM Journal on Matrix Analysis and Applications*, 34(4):1611–1630, 2013.

Bishop, C. M. *Pattern Recognition and Machine Learning (Information Science and Statistics)*. Springer-Verlag, Berlin, Heidelberg, 2006. ISBN 0387310738.

Bo, D., Wang, X., Shi, C., and Shen, H. Beyond low-frequency information in graph convolutional networks. In *AAAI*. AAAI Press, 2021.

Bruna, J., Zaremba, W., Szlam, A., and LeCun, Y. Spectral networks and locally connected networks on graphs. In *ICLR*, 2014.

Cai, C. and Wang, Y. A note on over-smoothing for graph neural networks. *arXiv:2006.13318*, 2020.

Chamberlain, B. P., Rowbottom, J., Eynard, D., Di Giovanni, F., Xiaowen, D., and Bronstein, M. M. Beltrami flow and neural diffusion on graphs. In *NeurIPS*, 2021a.

Chamberlain, B. P., Rowbottom, J., Goranova, M., Webb, S., Rossi, E., and Bronstein, M. M. Grand: Graph neural diffusion. In *ICML*, 2021b.

Chen, M., Wei, Z., Huang, Z., Ding, B., and Li, Y. Simple and deep graph convolutional networks. In III, H. D. and Singh, A. (eds.), *Proceedings of the 37th International Conference on Machine Learning*, volume 119 of *Proceedings of Machine Learning Research*, pp. 1725–1735. PMLR, 13–18 Jul 2020. URL <https://proceedings.mlr.press/v119/chen20v.html>.

Chien, E., Peng, J., Li, P., and Milenkovic, O. Adaptive universal generalized pagerank graph neural network. In *International Conference on Learning Representations*, 2021. URL <https://openreview.net/forum?id=n6j17fLxrP>.

Curry, J. M. *Sheaves, cosheaves and applications*. University of Pennsylvania, 2014.

Defferrard, M., Bresson, X., and Vandergheynst, P. Convolutional neural networks on graphs with fast localized spectral filtering. In *NIPS*, 2016.

Dwivedi, V. P., Joshi, C. K., Laurent, T., Bengio, Y., and Bresson, X. Benchmarking graph neural networks. *arXiv:2003.00982*, 2020.

Ghrist, R. and Riess, H. Cellular sheaves of lattices and the tarski laplacian. *arXiv:2007.04099*, 2020.

Gilmer, J., Schoenholz, S. S., Riley, P. F., Vinyals, O., and Dahl, G. E. Neural message passing for quantum chemistry. In *ICML*, 2017.

Goller, C. and Kuchler, A. Learning task-dependent distributed representations by backpropagation through structure. In *ICNN*, 1996.

Gori, M., Monfardini, G., and Scarselli, F. A new model for learning in graph domains. In *IJCNN*, 2005.

Hamilton, W. L., Ying, R., and Leskovec, J. Representation learning on graphs: Methods and applications. *IEEE Data Engineering Bulletin*, 2017.

Hansen, J. and Gebhart, T. Sheaf neural networks. In *NeurIPS 2020 Workshop on Topological Data Analysis and Beyond*, 2020.

Hansen, J. and Ghrist, R. Toward a spectral theory of cellular sheaves. *Journal of Applied and Computational Topology*, 3(4):315–358, 2019.

Hansen, J. and Ghrist, R. Opinion dynamics on discourse sheaves. *SIAM Journal on Applied Mathematics*, 81(5):2033–2060, 2021.

Hatcher, A. *Algebraic topology*. Cambridge Univ. Press, Cambridge, 2000.

Kingma, D. P. and Ba, J. Adam: A method for stochastic optimization. In *ICLR*, 2015.

Kipf, T. N. and Welling, M. Semi-supervised classification with graph convolutional networks. In *ICLR*, 2017.

Lee, H. D. On some matrix inequalities. *Korean Journal of Mathematics*, 16(4):565–571, 2008.

Lingam, V., Ragesh, R., Iyer, A., and Sellamanickam, S. Simple truncated svd based model for node classification on heterophilic graphs. *arXiv preprint arXiv:2106.12807*, 2021.

Mhammedi, Z., Hellicar, A., Rahman, A., and Bailey, J. Efficient orthogonal parametrisation of recurrent neural networks using householder reflections. In *International Conference on Machine Learning*, pp. 2401–2409. PMLR, 2017.

Nt, H. and Maehara, T. Revisiting graph neural networks: all we have is low pass filters. *arXiv preprint arXiv:1812.08434v4*, 2019.

Obukhov, A. Efficient householder transformation in pytorch, 2021. URL www.github.com/toshas/torch-householder. Version: 1.0.1, DOI: 10.5281/zenodo.5068733.

Oono, K. and Suzuki, T. Graph neural networks exponentially lose expressive power for node classification. *arXiv:1905.10947*, 2019.

Oono, K. and Suzuki, T. Graph neural networks exponentially lose expressive power for node classification. In *International Conference on Learning Representations*, 2020.

Paszke, A., Gross, S., Massa, F., Lerer, A., Bradbury, J., Chanan, G., Killeen, T., Lin, Z., Gimelshein, N., Antiga, L., Desmaison, A., Kopf, A., Yang, E., DeVito, Z., Raison, M., Tejani, A., Chilamkurthy, S., Steiner, B., Fang, L., Bai, J., and Chintala, S. Pytorch: An imperative style, high-performance deep learning library. In Wallach, H., Larochelle, H., Beygelzimer, A., d’Alché-Buc, F., Fox, E., and Garnett, R. (eds.), *Advances in Neural Information Processing Systems 32*, pp. 8024–8035. Curran Associates, Inc., 2019.

Pei, H., Wei, B., Chang, K. C.-C., Lei, Y., and Yang, B. Geom-gcn: Geometric graph convolutional networks. *arXiv preprint arXiv:2002.05287*, 2020.

Rozemberczki, B., Allen, C., and Sarkar, R. Multi-scale attributed node embedding. *Journal of Complex Networks*, 9(2):cnab014, 2021.

Scarselli, F., Gori, M., Tsoi, A. C., Hagenbuchner, M., and Monfardini, G. The graph neural network model. *IEEE Trans. Neural Networks*, 20(1):61–80, 2008.

Schafer, R. D. *An introduction to nonassociative algebras*. Courier Dover Publications, 2017.

Singer, A. and Wu, H.-T. Vector diffusion maps and the connection laplacian. *Communications on pure and applied mathematics*, 65(8):1067–1144, 2012.

Sperduti, A. Encoding labeled graphs by labeling RAAM. In *NIPS*, 1994.

Tu, L. W. Manifolds. In *An Introduction to Manifolds*, pp. 47–83. Springer, 2011.

Veličković, P., Cucurull, G., Casanova, A., Romero, A., Lio, P., and Bengio, Y. Graph attention networks. In *ICLR*, 2018.

Xhonneux, L.-P., Qu, M., and Tang, J. Continuous graph neural networks. In *ICML*, 2020.

Yan, Y., Hashemi, M., Swersky, K., Yang, Y., and Koutra, D. Two sides of the same coin: Heterophily and oversmoothing in graph convolutional neural networks. *arXiv:2102.06462*, 2021.

Zhao, L. and Akoglu, L. Pairnorm: Tackling oversmoothing in gnns. In *International Conference on Learning Representations*, 2020. URL <https://openreview.net/forum?id=rkecl1rtwB>.

Zhu, J., Yan, Y., Zhao, L., Heimann, M., Akoglu, L., and Koutra, D. Beyond homophily in graph neural networks: Current limitations and effective designs. *Advances in Neural Information Processing Systems*, 33, 2020.

A. Harmonic Space Proofs

Proof of Proposition 7. We first note that on a discrete $O(d)$ bundle the degree operator $D_v = d_v \mathbf{I}$ since by orthogonality $\mathcal{F}_{v \leq e}^\top \mathcal{F}_{v \leq e} = \mathbf{I}$. We can use the Rayleigh quotient to characterize $\lambda_0^{\mathcal{F}}$ as

$$\lambda_0^{\mathcal{F}} = \min_{\mathbf{x} \in \mathbb{R}^{nd}} \frac{\langle \mathbf{x}, \Delta_{\mathcal{F}} \mathbf{x} \rangle}{\|\mathbf{x}\|^2}.$$

Fix $v \in V$ and choose a minimal path $\gamma_{v \rightarrow u}$ for all $u \in V$. For an arbitrary non-zero \mathbf{z}_v , consider the signal $\mathbf{z}_u = P_{v \rightarrow u}^\gamma \mathbf{z}_v$ and we set $\tilde{\mathbf{z}}_u \sqrt{d_u} = \mathbf{z}_u$.

$$\|\mathcal{F}_{u \leq e} \frac{\mathbf{z}_u}{\sqrt{d_u}} - \mathcal{F}_{w \leq e} \frac{\mathbf{z}_w}{\sqrt{d_w}}\|^2 = \|\tilde{\mathbf{z}}_u - (\mathcal{F}_{u \leq e}^\top \mathcal{F}_{w \leq e}) \tilde{\mathbf{z}}_w\|^2 = \|P_{v \rightarrow u}^\gamma \tilde{\mathbf{z}}_v - (\mathcal{F}_{u \leq e}^\top \mathcal{F}_{w \leq e}) \mathbf{P}_{v \rightarrow w}^\gamma \tilde{\mathbf{z}}_v\|^2,$$

where we have again used that the maps are orthogonal. Since $(\mathcal{F}_{u \leq e}^\top \mathcal{F}_{w \leq e}) \mathbf{P}_{v \rightarrow w}^\gamma = \mathbf{P}_{v \rightarrow u}^{\gamma'}$ we find that the right hand side can be bound from above by $r^2 \|\tilde{\mathbf{z}}_v\|^2$. Therefore, by using Definition 24 we finally obtain

$$\lambda_0^{\mathcal{F}} = \min_{\mathbf{x} \in \mathbb{R}^{nd}} \frac{\langle \mathbf{x}, \Delta_{\mathcal{F}} \mathbf{x} \rangle}{\|\mathbf{x}\|^2} \leq \frac{\langle \mathbf{z}, \Delta_{\mathcal{F}} \mathbf{z} \rangle}{\|\mathbf{z}\|^2} = \frac{1}{2} \frac{\sum_{u \sim w} \|\mathcal{F}_{u \leq e} \frac{\mathbf{z}_u}{\sqrt{d_u}} - \mathcal{F}_{w \leq e} \frac{\mathbf{z}_w}{\sqrt{d_w}}\|^2}{\|\mathbf{z}\|^2} \leq \frac{r^2}{2} \frac{\sum_{u \sim w} \|\tilde{\mathbf{z}}_v\|^2}{\|\mathbf{z}\|^2}.$$

Since the transport maps are all orthogonal we get

$$\|\mathbf{z}\|^2 = \sum_u d_u \|\mathbf{P}_{v \rightarrow u}^\gamma \tilde{\mathbf{z}}_v\|^2 = \sum_u d_u \|\tilde{\mathbf{z}}_v\|^2 = \sum_{u \sim w} \|\tilde{\mathbf{z}}_v\|^2.$$

We conclude that

$$\lambda_0^{\mathcal{F}} \leq \frac{r^2}{2} \frac{\sum_{u \sim w} \|\tilde{\mathbf{z}}_v\|^2}{\|\mathbf{z}\|^2} = \frac{r^2}{2}.$$

□

Proof of Proposition 8. Assume that $\mathbf{x} \in H^0(G, \mathcal{F})$ and consider $v \in V$ and any cycle based at v denoted by $\gamma_{v \rightarrow v} = (v_0 = v, v_1, \dots, v_L = v)$. According to Theorem 6 we have that

$$\mathcal{F}_{v_{i+1} \leq e} \mathbf{x}_{v_{i+1}} = \mathcal{F}_{v_i \leq e} \mathbf{x}_{v_i} \implies \mathbf{x}_{v_{i+1}} = (\mathcal{F}_{v_{i+1}}^\top \mathcal{F}_{v_i}) \mathbf{x}_{v_i} := \rho_{v_i \rightarrow v_{i+1}} \mathbf{x}_{v_i}.$$

By composing all the maps we find:

$$\mathbf{x}_v = \rho_{v_{L-1} \rightarrow v_L} \cdots \rho_{v_0 \rightarrow v_1} \mathbf{x}_v = \mathbf{P}_{v \rightarrow v}^\gamma \mathbf{x}_v$$

which completes the proof. □

Proof of Proposition 9. If $\epsilon = 0$ there is nothing to prove. Assume that $\epsilon > 0$. By Proposition 8 we derive that the harmonic space is trivial and hence $\lambda_0^{\mathcal{F}} > 0$. Consider a unit eigenvector $\mathbf{x} \in \ker(\Delta_{\mathcal{F}} - \lambda_0^{\mathcal{F}} \mathbf{I})$ and let $v \in V$ such that $\|\mathbf{x}_v\| \geq \|\mathbf{x}_u\|$ for $u \neq v$. There exists a cycle γ based at v such that $\mathbf{P}_v^\gamma \mathbf{x}_v \neq \mathbf{x}_v$ for otherwise we could extend $\mathbf{x}_v \neq 0$ to any other node independently of the path choice and hence find a non-trivial harmonic signal. In particular, we can assume this cycle to be non-degenerate, otherwise if there existed a non-trivial degenerate loop contained in γ that does not fix \mathbf{x} we could consider this loop instead of γ for our argument. Let us write this path as $(v_0 = v, v_1, \dots, v_L = v)$ and consider the rescaled signal $\tilde{\mathbf{x}}_v \sqrt{d_v} = \mathbf{x}_v$. By assumption we have

$$\begin{aligned} \epsilon \|\tilde{\mathbf{x}}_v\| &\leq \|(\mathbf{P}_{v \rightarrow v}^\gamma - \mathbf{I}) \tilde{\mathbf{x}}_v\| = \|(\rho_{v_{L-1} \rightarrow v_L} \cdots \rho_{v_0 \rightarrow v_1} - \mathbf{I}) \tilde{\mathbf{x}}_v\| \\ &= \|\mathcal{F}_{v_{L-1}} \rho_{v_{L-2} \rightarrow v_{L-1}} \cdots \rho_{v_0 \rightarrow v_1} \tilde{\mathbf{x}}_v - \mathcal{F}_{v_L=v} \tilde{\mathbf{x}}_v\| \\ &= \|\mathcal{F}_{v_{L-1}} \rho_{v_{L-2} \rightarrow v_{L-1}} \cdots \rho_{v_0 \rightarrow v_1} \tilde{\mathbf{x}}_v - \mathcal{F}_{v_{L-1}} \tilde{\mathbf{x}}_{v_{L-1}} + \mathcal{F}_{v_{L-1}} \tilde{\mathbf{x}}_{v_{L-1}} - \mathcal{F}_{v_L=v} \tilde{\mathbf{x}}_v\| \\ &\leq \|\rho_{v_{L-2} \rightarrow v_{L-1}} \cdots \rho_{v_0 \rightarrow v_1} \tilde{\mathbf{x}}_v - \tilde{\mathbf{x}}_{v_{L-1}}\| + \|\mathcal{F}_{v_{L-1}} \tilde{\mathbf{x}}_{v_{L-1}} - \mathcal{F}_{v_L=v} \tilde{\mathbf{x}}_v\|. \end{aligned}$$

By iterating the approach above we find:

$$\begin{aligned} \epsilon \|\tilde{\mathbf{x}}_v\| &\leq \sum_{i=0}^L \|\mathcal{F}_{v_i} \tilde{\mathbf{x}}_{v_i} - \mathcal{F}_{v_{i+1}} \tilde{\mathbf{x}}_{v_{i+1}}\| \leq \sqrt{L} \left(\sum_{i=0}^L \|\mathcal{F}_{v_i} \tilde{\mathbf{x}}_{v_i} - \mathcal{F}_{v_{i+1}} \tilde{\mathbf{x}}_{v_{i+1}}\|^2 \right)^{\frac{1}{2}} \\ &= \sqrt{L} \left(\sum_{i=0}^L \left\| \mathcal{F}_{v_i} \frac{\mathbf{x}_{v_i}}{\sqrt{d_{v_i}}} - \mathcal{F}_{v_{i+1}} \frac{\mathbf{x}_{v_{i+1}}}{\sqrt{d_{v_{i+1}}}} \right\|^2 \right)^{\frac{1}{2}}. \end{aligned}$$

From Definition 24 we derive that the last term can be bounded from above by $\sqrt{2L E_{\mathcal{F}}(\mathbf{x})} = \sqrt{2L \langle \mathbf{x}, \Delta_{\mathcal{F}} \mathbf{x} \rangle}$. Therefore, we conclude:

$$\epsilon \frac{\|\mathbf{x}_v\|}{\sqrt{d_v}} \leq \sqrt{2L \langle \mathbf{x}, \Delta_{\mathcal{F}} \mathbf{x} \rangle} = \sqrt{2L \lambda_0^{\mathcal{F}}} \|\mathbf{x}\| \leq 2\sqrt{\text{diam}(G) \lambda_0^{\mathcal{F}}}.$$

By construction we get $\|\mathbf{x}_v\| \geq 1/\sqrt{n}$, meaning that

$$\lambda_0^{\mathcal{F}} \geq \frac{\epsilon^2}{2\text{diam}(G)} \frac{1}{n d_{\max}}.$$

□

Proof of Lemma 10. We first note that the argument below extends to weighted $O(d)$ -bundles as well. Let $\mathbf{x} \in H^0(G, \mathcal{F})$. According to Proposition 8, given $v, u \in V$, we see that $x_u = \mathbf{P}_{v \rightarrow u}^{\gamma} x_v$ for any path $\gamma_{v \rightarrow u}$. It means that the harmonic space is uniquely determined by the choice of $\mathbf{x}_v \in \mathcal{F}(v)$. Explicitly, given any cycle γ based at v , we know that $\mathbf{x}_v \in \ker(\mathbf{P}_{v \rightarrow v}^{\gamma} - I)$. If the transport is everywhere path-independent, then the kernel coincides with the whole stalk $\mathcal{F}(v)$ and hence we can extend any basis $\{\mathbf{x}_{v_i}\} \in \mathcal{F}(v) \cong \mathbb{R}^d$ to a basis in $H^0(G, \mathcal{F})$ via the transport maps, i.e. $\dim(H^0(G, \mathcal{F})) = d$. If instead there exists a transport map over a cycle $\gamma_{v \rightarrow v}$ with non-trivial fixed points, then $\ker(\mathbf{P}_{v \rightarrow v}^{\gamma} - I) < \mathcal{F}(v) \cong \mathbb{R}^d$ and hence $\dim(H^0(G, \mathcal{F})) < d$. □

B. Proofs for the Power of Sheaf Diffusion

Definition 29. Let $G = (V, \mathbf{W})$ be a weighted graph, where \mathbf{W} is a matrix with $w_{vu} = w_{uv} \geq 0$ for all $v \neq u \in V$, $w_{vv} = 0$ for all $v \in V$, and (v, u) is an edge if and only if $w_{vu} > 0$.

The graph Laplacian of a weighted graph is $\mathbf{L} = \mathbf{D} - \mathbf{W}$, where \mathbf{D} is the diagonal matrix of weighted degrees (i.e. $d_v = \sum_u w_{vu}$). Its normalised version is $\tilde{\mathbf{L}} = \mathbf{D}^{-1/2} \mathbf{L} \mathbf{D}^{-1/2}$.

Proposition 30. Let G be a graph. The set $\{\Delta_{\mathcal{F}} \mid (G, \mathcal{F}) \in \mathcal{H}_{\text{sym}}^1\}$ is isomorphic to the set of all possible weighted graph Laplacians over G .

Proof. We prove only one direction. Let \mathbf{W} be a choice of valid weight matrix for the graph G . We can construct a sheaf $(G, \mathcal{F}) \in \mathcal{H}_{\text{sym}}^1$ such that for all edges $v, u \trianglelefteq e$ we have that $\mathcal{F}_{v \trianglelefteq e} = \mathcal{F}_{u \trianglelefteq e} = \pm \sqrt{w_{vu}}$. Then, $\mathcal{L}_{vu} = -w_{vu}$ and $\mathcal{L}_{vv} = \sum_e \|\mathcal{F}_{v \trianglelefteq e}\|^2 = \sum_u w_{vu}$. The equality for the normalised version of the Laplacians follows directly. □

We state the following Lemma without proof based on Theorem 3.1 in Hansen & Ghrist (2021).

Lemma 31. Solutions $\mathbf{X}(t)$ to the diffusion in Equation 1 converge as $t \rightarrow \infty$ to the orthogonal projection of $\mathbf{X}(0)$ onto $\ker(\Delta_{\mathcal{F}})$.

Due to this Lemma, the proofs below rely entirely on the structure of $\ker(\Delta_{\mathcal{F}})$ that one obtains for certain (G, \mathcal{F}) .

Proof of Proposition 13. Let $G = (V, E)$ be a graph with two classes $A, B \subset V$ such that for each $v \in A$, there exists $u \in A$ and an edge $(v, u) \in E$. Additionally, let $\mathbf{x}(0)$ be any channel of the feature matrix $\mathbf{X}(0) \in \mathbb{R}^{n \times f}$.

We can construct a sheaf $(\mathcal{F}, G) \in \mathcal{H}_{\text{sym}}^1$ as follows. For all nodes $v \in V$ and edges $e \in E$, $\mathcal{F}(v) \cong \mathcal{F}(e) \cong \mathbb{R}$. For all $v, u \in A$ and edge $(u, v) \in E$, set $\mathcal{F}_{v \trianglelefteq e} = \mathcal{F}_{u \trianglelefteq e} = \sqrt{\alpha} > 0$. Otherwise, set $\mathcal{F}_{v \trianglelefteq e} = 1$.

Denote by h_v the number of neighbours of node v in the same class as v . Note that based on the assumptions, $h_v > 1$ if $v \in A$. Then the only harmonic eigenvector of $\Delta_{\mathcal{F}}$ is:

$$\mathbf{a}_v = \begin{cases} \sqrt{d_v + h_v(\alpha - 1)}, & v \in A \\ \sqrt{d_v}, & v \in B \end{cases} \quad (7)$$

Denote its unit-normalised version $\tilde{\mathbf{a}} := \frac{\mathbf{a}}{\|\mathbf{a}\|}$. In the limit of the diffusion process, the features converge to $\mathbf{h} = \langle \mathbf{x}(0), \tilde{\mathbf{a}} \rangle \tilde{\mathbf{a}}$ by Lemma 31. Assuming, $\mathbf{x}(0) \notin \ker(\Delta_{\mathcal{F}})^\perp$, which is nowhere dense in \mathbb{R}^n and, without loss of generality, that $\langle \mathbf{x}(0), \tilde{\mathbf{a}} \rangle > 0$, for sufficiently large α , $\tilde{\mathbf{a}}_v \geq \tilde{\mathbf{a}}_u$ for all $v \in A, u \in B$. \square

Proof of Proposition 14. Let $G = (A, B, E)$ be a bipartite graph with $|A| = |B|$ and let $\mathbf{x}(0) \in \mathbb{R}^n$ be any channel of the feature matrix $\mathbf{X}(0) \in \mathbb{R}^{n \times f}$.

Consider an arbitrary sheaf $(G, \mathcal{F}) \in \mathcal{H}_{\text{sym}}^1$. Since the graph is connected, the only harmonic eigenvector of $\Delta_{\mathcal{F}}$ is $\mathbf{y} \in \mathbb{R}^n$ with $\mathbf{y}_v = \sqrt{\sum_{v \leq e} \|\mathcal{F}_{v \leq e}\|^2}$ (i.e. the square root of the weighted degree). Based on Lemma 31, the diffusion process converges in the limit (up to a scaling) to $\langle \mathbf{x}, \mathbf{y} \rangle \mathbf{y}$. For the features to be linearly separable we require that $\langle \mathbf{x}, \mathbf{y} \rangle \neq 0$ and, without loss of generality, for all $v \in A, u \in B$ that $\mathbf{y}_v < \mathbf{y}_u \Leftrightarrow \sum_{v \leq e} \|\mathcal{F}_{v \leq e}\|^2 < \sum_{u \leq e} \|\mathcal{F}_{u \leq e}\|^2$.

Suppose for the sake of contradiction there exists a sheaf in $\mathcal{H}_{\text{sym}}^1$ with such a harmonic eigenvector. Then, because $|A| = |B|$:

$$\sum_{v \in A} \sum_{v \leq e} \|\mathcal{F}_{v \leq e}\|^2 < \sum_{u \in B} \sum_{u \leq e} \|\mathcal{F}_{u \leq e}\|^2 \Leftrightarrow \sum_{v \in A} \sum_{v \leq e} \|\mathcal{F}_{v \leq e}\|^2 - \sum_{u \in B} \sum_{u \leq e} \|\mathcal{F}_{u \leq e}\|^2 < 0 \Leftrightarrow \sum_{e \in E} \|\mathcal{F}_{v \leq e}\|^2 - \|\mathcal{F}_{u \leq e}\|^2 < 0$$

However, because $(\mathcal{F}, G) \in \mathcal{H}_{\text{sym}}^1$, we have $\mathcal{F}_{v \leq e} = \mathcal{F}_{u \leq e}$ and the sum above is zero. \square

Proof of Proposition 16. Let $G = (V, E)$ be a connected graph with two classes $A, B \subset V$. Additionally, let $\mathbf{x}(0)$ be any channel of the feature matrix $\mathbf{X}(0) \in \mathbb{R}^{n \times f}$.

We can construct a sheaf $(\mathcal{F}, G) \in \mathcal{H}^1(G)$ as follows. For all nodes v and edges e , $\mathcal{F}(v) \cong \mathcal{F}(e) \cong \mathbb{R}$. For all $v \in A$, set $\mathcal{F}_{v \leq e} = \alpha$. For all $u \in B$, set $\mathcal{F}_{u \leq e} = \beta$. Additionally, let $\alpha < 0 < \beta$.

Since the graph is connected, by Lemma 10, the only harmonic eigenvector of $\Delta_{\mathcal{F}}$ is:

$$\mathbf{y}_v = \begin{cases} \beta \sqrt{\sum_{v \leq e} \alpha^2} & v \in A \\ \alpha \sqrt{\sum_{v \leq e} \beta^2} & v \in B \end{cases} = \begin{cases} \beta |\alpha| \sqrt{d_v}, & v \in A \\ \alpha |\beta| \sqrt{d_v}, & v \in B \end{cases} \quad (8)$$

Assume $\mathbf{x}(0) \notin \ker(\Delta_{\mathcal{F}})^\perp$, which is nowhere dense in \mathbb{R}^n and, without loss of generality, that $\langle \mathbf{x}(0), \mathbf{y} \rangle > 0$. Then, $\mathbf{y}_v > 0 > \mathbf{y}_u$ for all $v \in A, u \in B$. \square

Proof of Proposition 18. Let G be the connected graph with two nodes $V = \{v, u\}$. Then any sheaf $(\mathcal{F}, G) \in \mathcal{H}_+^1(G)$ has restriction maps of the form $\mathcal{F}_{v \leq e} = \alpha, \mathcal{F}_{u \leq e} = \beta$ and (without loss of generality) $\alpha, \beta > 0$. As before, the only (unnormalised) harmonic eigenvector for a sheaf of this form is $\mathbf{y} = (|\alpha|/\beta, |\alpha|/\beta) = (\alpha\beta, \alpha\beta)$. Since this is a constant vector, the two nodes are not separable in the diffusion limit. \square

We state the following result without proof (see Exercise 4.1 in Bishop (2006)).

Lemma 32. Let A and B be two sets of points in \mathbb{R}^n . If their convex hulls intersect, the two sets of points cannot be linearly separable.

Proof of Proposition 19. If the sheaf has a trivial global section, then all features converge to zero in the diffusion limit. Suppose $H^0(G, \mathcal{F})$ is non-trivial. Since G is connected and all the restriction maps are invertible, by Lemma 10, $\dim(H^0) = 1$.

In that case, let \mathbf{h} be the unit-normalised harmonic eigenvector of $\Delta_{\mathcal{F}}$. By Lemma 31, for any node v , its scalar feature in channel $k \leq f$ is given by $x_v^k(\infty) = \langle \mathbf{x}^k(0), \mathbf{h} \rangle \mathbf{h}_v$. Note that we can always find three nodes v, u, w belonging to three

different classes such that $\mathbf{h}_v \leq \mathbf{h}_u \leq \mathbf{h}_w$. Then, there exists a convex combination $\mathbf{h}_u = \alpha \mathbf{h}_v + (1 - \alpha) \mathbf{h}_w$, with $\alpha \in [0, 1]$. Therefore:

$$\mathbf{x}_u^k(\infty) = \langle \mathbf{x}^k(0), \mathbf{h} \rangle \mathbf{h}_u = \alpha \langle \mathbf{x}^k(0), \mathbf{h} \rangle \mathbf{h}_v + (1 - \alpha) \langle \mathbf{x}^k(0), \mathbf{h} \rangle \mathbf{h}_w = \alpha \mathbf{x}_v^k(\infty) + (1 - \alpha) \mathbf{x}_w^k(\infty). \quad (9)$$

Since this is true for all channels $k < f$, it follows that $\mathbf{x}_u(\infty) = \alpha \mathbf{x}_v(\infty) + (1 - \alpha) \mathbf{x}_w(\infty)$. Because $\mathbf{x}_u(\infty)$ is in the convex hull of the points belonging to other classes, by Lemma 32, the class of v is not linearly separable from the other classes. \square

Proof of Proposition 21. Let $G = (V, E)$ be a connected graph with C classes and (\mathcal{F}, G) , an arbitrary sheaf in $\mathcal{H}^C(G)$. Because \mathcal{F} has diagonal restriction maps there is no interaction during diffusion between the different dimensions of the stalks. Therefore, the diffusion process can be written as d independent diffusion processes, where the i -th process uses a sheaf \mathcal{F}^i with all stalks isomorphic to \mathbb{R} and $\mathcal{F}_{v \leq e}^i = \mathcal{F}_{v \leq e}(i, i)$ for all $v \in V$ and incident edges e . Therefore, we can construct d sheaves $\mathcal{F}^i \in \mathcal{H}^1(G)$ with $i < d$ as in Proposition 16, where (in one vs all fashion) the two classes are given by the nodes in class i and the nodes belonging to the other classes.

It remains to restrict that the projection of $\mathbf{x}(0)$ on any of the harmonic eigenvectors of $\Delta_{\mathcal{F}}$ in the standard basis is non-zero. Formally, we require $\mathbf{x}^i(0) \notin \ker(\Delta_{\mathcal{F}^i})^\perp$ for all positive integers $i \leq d$. Since $\ker(\Delta_{\mathcal{F}^i})^\perp$ is nowhere dense in \mathbb{R}^n , $\mathbf{x}(0)$ belongs to the direct sum of dense subspaces, which is dense. \square

Lemma 33. Let $G = (V, E)$ be a graph and (\mathcal{F}, G) a (weighted) orthogonal vector bundle over G with path-independent parallel transport and edge weights α_e . Consider an arbitrary node $v^* \in V$ and denote by \mathbf{e}_i the i -th standard basis vector of \mathbb{R}^d . Then $\{\mathbf{h}^1, \dots, \mathbf{h}^d\}$ form an orthogonal eigenbasis for the harmonic space of $\Delta_{\mathcal{F}}$, where:

$$\mathbf{h}_v^i = \begin{cases} \mathbf{e}_i \sqrt{d_v^{\mathcal{F}}} & v = v^* \\ \mathbf{P}_{v \rightarrow w} \mathbf{e}_i \sqrt{d_v^{\mathcal{F}}} & \text{otherwise} \end{cases} = \begin{cases} \mathbf{e}_i \sqrt{\sum_{v \leq e} \alpha_e^2}, & v = v^* \\ \mathbf{P}_{v^* \rightarrow w} \mathbf{e}_i \sqrt{\sum_{v \leq e} \alpha_e^2}, & \text{otherwise} \end{cases} \quad (10)$$

Proof. First, we show that \mathbf{h}_v^i is harmonic.

$$E_{\mathcal{F}}(\mathbf{h}_v^i) = \frac{1}{2} \sum_{v, u, e:=(v, u)} \left\| \frac{1}{\sqrt{d_v^{\mathcal{F}}}} \mathcal{F}_{v \leq e} \mathbf{h}_v - \frac{1}{\sqrt{d_u^{\mathcal{F}}}} \mathcal{F}_{u \leq e} \mathbf{h}_u \right\|_2^2 \quad (11)$$

$$= \frac{1}{2} \sum_{v, u, e:=(v, u)} \left\| \mathcal{F}_{v \leq e} \mathbf{P}_{v^* \rightarrow v} \mathbf{e}_i - \mathcal{F}_{u \leq e} \mathbf{P}_{v^* \rightarrow u} \mathbf{e}_i \right\|_2^2 \quad (12)$$

$$= \frac{1}{2} \sum_{v, u, e:=(v, u)} \left\| \mathcal{F}_{v \leq e} \mathbf{P}_{u \rightarrow v} \mathbf{P}_{v^* \rightarrow u} \mathbf{e}_i - \mathcal{F}_{u \leq e} \mathbf{P}_{v^* \rightarrow u} \mathbf{e}_i \right\|_2^2 \quad \text{By path independence} \quad (13)$$

$$= \frac{1}{2} \sum_{v, u, e:=(v, u)} \left\| \mathcal{F}_{v \leq e} \mathcal{F}_{v \leq e}^{\top} \mathcal{F}_{u \leq e} \mathbf{P}_{v^* \rightarrow u} \mathbf{e}_i - \mathcal{F}_{u \leq e} \mathbf{P}_{v^* \rightarrow u} \mathbf{e}_i \right\|_2^2 \quad \text{By definition of } \mathbf{P}_{u \rightarrow v} \quad (14)$$

$$= \frac{1}{2} \sum_{v, u, e:=(v, u)} \left\| \mathcal{F}_{u \leq e} \mathbf{P}_{v^* \rightarrow u} \mathbf{e}_i - \mathcal{F}_{u \leq e} \mathbf{P}_{v^* \rightarrow u} \mathbf{e}_i \right\|_2^2 = 0 \quad \text{Orthogonality of } \mathcal{F}_{v \leq e} \quad (15)$$

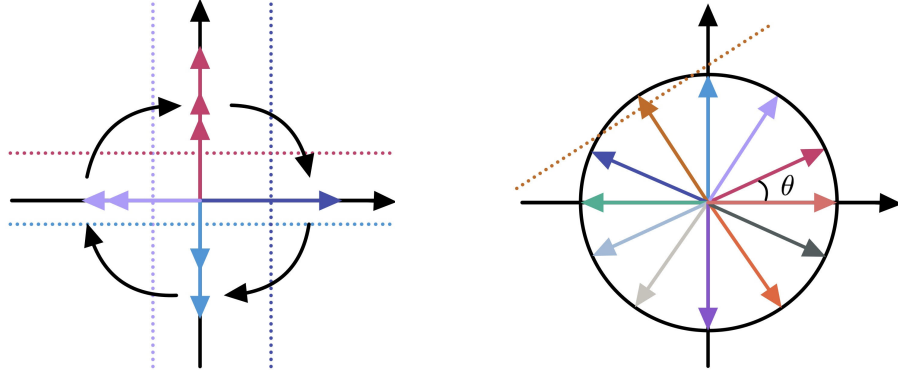
For orthogonality, notice that for any $i, j \leq d$ and $v \in V$, it holds that:

$$\langle \mathbf{h}_v^i, \mathbf{h}_v^j \rangle = \langle \mathbf{P}_{v^* \rightarrow w} \mathbf{e}_i \sqrt{d_v^{\mathcal{F}}}, \mathbf{P}_{v^* \rightarrow w} \mathbf{e}_j \sqrt{d_v^{\mathcal{F}}} \rangle = \sqrt{d_v^{\mathcal{F}}} \sqrt{d_v^{\mathcal{F}}} \langle \mathbf{e}_i, \mathbf{e}_j \rangle = 0 \quad (16)$$

\square

Lemma 34. Let $\mathbf{R}_1, \mathbf{R}_2$ be two 2D rotation matrices and $\mathbf{e}_1, \mathbf{e}_2$ the two standard basis vectors of \mathbb{R}^2 . Then $\langle \mathbf{R}_1 \mathbf{e}_1, \mathbf{R}_2 \mathbf{e}_2 \rangle = -\langle \mathbf{R}_1 \mathbf{e}_2, \mathbf{R}_2 \mathbf{e}_1 \rangle$.

Proof. The angle between \mathbf{e}_1 and \mathbf{e}_2 is $\frac{\pi}{2}$. Letting ϕ, θ be the positive rotation angles of the two matrices, the first inner product is equal to $\cos(\pi/2 + (\phi - \theta))$ while the second is $\cos(\pi/2 - (\phi - \theta))$. The result follows from applying the trigonometric identity $\cos(\pi/2 + x) = -\sin x$. \square



(a) Aligning the features of each class with the axis of coordinates in a 2D space. Dotted lines indicate linear decision boundaries for each class.

(b) Separating an arbitrary number of classes when the graph is regular. Dotted line shows an example decision boundary for one of the classes.

Figure 4. Proof sketch for Lemma 35 and Proposition 36.

We first prove Theorem 23 in dimension two in the following lemma and then we will look at the general case.

Lemma 35. *Let \mathcal{G} be the class of connected graphs with $C \leq 4$ classes. Then, $\mathcal{H}_{\text{orth}}^2(G)$ has linear separation power over \mathcal{G} .*

Proof. Idea: We can use rotation matrices to align the harmonic features of the classes with the axis of coordinates as in Figure 4a. Then, for each side of each axis, we can find a separating hyperplane separating each class from all the others.

Let G be a connected graph with $C \leq 4$ classes. Denote by \mathcal{P} the following set of rotation matrices together with their signed-flipped counterparts:

$$\mathbf{R}_1 = \begin{bmatrix} 1 & 0 \\ 0 & 1 \end{bmatrix}, \quad \mathbf{R}_2 = \begin{bmatrix} 0 & -1 \\ 1 & 0 \end{bmatrix} \quad (17)$$

and by $\mathcal{C} = \{1, \dots, C\}$ the set of all class labels. Then, fix a node $v^* \in V$ and construct an injective map $g : \mathcal{C} \rightarrow \mathcal{P}$ assigning each class label one of the signed basis vectors such that $g(c(v^*)) = \mathbf{R}_1$, where $c(v^*)$ denotes the class of node v^* .

Then, we can construct an sheaf $(G, \mathcal{F}) \in \mathcal{H}_{\text{orth}}^2(G)$ in terms of certain parallel transport maps along each edge, that will depend on \mathcal{P} . For all nodes v and edges e , $\mathcal{F}(v) \cong \mathcal{F}(e) \cong \mathbb{R}^2$. For each $u \in V$, we set $\mathbf{P}_{v^* \rightarrow u} = g(c(u))$. Then for all $v, u \in V$, set $\mathbf{P}_{v \rightarrow u} = \mathbf{P}_{v^* \rightarrow v} \mathbf{P}_{u \rightarrow v}^{-1}$. It is easy to see that the resulting parallel transport is path-independent because it depends purely on the classes of the endpoints of the path.

Based on Lemma 33, the i -th eigenvector of $\Delta_{\mathcal{F}}$ is $\mathbf{h}^i \in \mathbb{R}^{2 \times n}$ with $\mathbf{h}_u^i = \mathbf{P}_{v^* \rightarrow u} \mathbf{e}_i \sqrt{d_u}$. Now we will show that the projection of $\mathbf{x}(0)$ in this subspace will have a configuration as in Figure 4a up to a rotation.

Let u, w be two nodes belonging to two different classes. Denote by $\alpha_i = \langle \mathbf{x}(0), \mathbf{h}^i \rangle$. Then the inner product between the features of nodes u, w in the limit of the diffusion process is:

$$\begin{aligned} & \langle \mathbf{P}_{v^* \rightarrow u} \sum_i \alpha_i \mathbf{e}_i \sqrt{d_u}, \mathbf{P}_{v^* \rightarrow w} \sum_j \alpha_j \mathbf{e}_j \sqrt{d_w} \rangle = \\ &= \sqrt{d_u d_w} \left[\sum_{i \neq j} \alpha_i \alpha_j \langle \mathbf{P}_{v^* \rightarrow u} \mathbf{e}_i, \mathbf{P}_{v^* \rightarrow w} \mathbf{e}_j \rangle + \sum_k \alpha_k^2 \langle \mathbf{P}_{v^* \rightarrow u} \mathbf{e}_k, \mathbf{P}_{v^* \rightarrow w} \mathbf{e}_k \rangle \right] \\ &= \sqrt{d_u d_w} \left[\sum_{i < j} \alpha_i \alpha_j \left(\langle \mathbf{P}_{v^* \rightarrow u} \mathbf{e}_i, \mathbf{P}_{v^* \rightarrow w} \mathbf{e}_j \rangle + \langle \mathbf{P}_{v^* \rightarrow u} \mathbf{e}_j, \mathbf{P}_{v^* \rightarrow w} \mathbf{e}_i \rangle \right) + \sum_k \alpha_k^2 \langle \mathbf{P}_{v^* \rightarrow u} \mathbf{e}_k, \mathbf{P}_{v^* \rightarrow w} \mathbf{e}_k \rangle \right] \quad (18) \\ &= \sum_k \alpha_k^2 \langle \mathbf{P}_{v^* \rightarrow u} \mathbf{e}_k, \mathbf{P}_{v^* \rightarrow w} \mathbf{e}_k \rangle \end{aligned}$$

(by Lemma 34)

It can be checked that by substituting the transport maps $\mathbf{P}_{v^* \rightarrow u}, \mathbf{P}_{v^* \rightarrow w}$ with any $\mathbf{R}_a, \mathbf{R}_b$ from \mathcal{P} such that $\mathbf{R}_a \neq \pm \mathbf{R}_b$, the inner product above is zero. Similarly, substituting any $\mathbf{R}_a = -\mathbf{R}_b$, the inner product is $-\sqrt{d_u d_w} \sum_k \alpha_k^2 = -\sqrt{d_u d_w} \|\mathbf{x}(0)\|^2$, which is equal to the product of the norms of the two vectors. Therefore, the diffused features of different classes are positioned at $\frac{\pi}{2}, \pi, \frac{3\pi}{2}$ from each other, as in Figure 4a. \square

Proof of Theorem 23. To generalise the proof, we need to find a set \mathcal{P} of size d containing rotation matrices that make the projected features of different classes be pairwise orthogonal for any projection coefficients α . For that, each term in Equation 18 must be zero for any coefficients α .

Therefore, $\mathcal{P} = \{\mathbf{P}_0, \dots, \mathbf{P}_{d-1}\}$ must satisfy the following requirements:

1. $\mathbf{P}_0 = \mathbf{I} \in \mathcal{P}$, since transport for neighbours in the same class must be the identity. Therefore, $\mathbf{P}_0 \mathbf{P}_k = \mathbf{P}_k \mathbf{P}_0 = \mathbf{P}_k$ for all k .
2. Since $\langle \mathbf{P}_0 \mathbf{e}_i, \mathbf{P}_k \mathbf{e}_i \rangle = 0$ for all i and $k \neq 0$, it follows that the diagonal elements of \mathbf{P}_k are zero.
3. From $\langle \mathbf{P}_0 \mathbf{e}_i, \mathbf{P}_k \mathbf{e}_j \rangle = -\langle \mathbf{P}_0 \mathbf{e}_j, \mathbf{P}_k \mathbf{e}_i \rangle$ for all $i \neq j, k \neq 0$ and point (2) it follows that $\mathbf{P}_k^{-1} = \mathbf{P}_k^\top = -\mathbf{P}_k$. Therefore, $\mathbf{P}_k \mathbf{P}_k = -\mathbf{I}$ for all $k \neq 0$.
4. We have $\langle \mathbf{P}_k \mathbf{e}_i, \mathbf{P}_l \mathbf{e}_i \rangle = 0$ for all i and $k \neq l$. Together with (3), it follows that the diagonal elements of $\mathbf{P}_k \mathbf{P}_l$ are zero.
5. We have $\langle \mathbf{P}_k \mathbf{e}_i, \mathbf{P}_l \mathbf{e}_j \rangle = -\langle \mathbf{P}_k \mathbf{e}_j, \mathbf{P}_l \mathbf{e}_i \rangle$ for all $i \neq j$, and $k \neq l$, with $k, l \neq 0$. Together with point (4) it follows that $(\mathbf{P}_k \mathbf{P}_l)^\top = -\mathbf{P}_k \mathbf{P}_l$. Similarly, from point (3) we have that $(\mathbf{P}_k \mathbf{P}_l)^\top = \mathbf{P}_l^\top \mathbf{P}_k^\top = (-\mathbf{P}_l)(-\mathbf{P}_k) = \mathbf{P}_l \mathbf{P}_k$. Therefore, the two matrices are anti-commutative: $\mathbf{P}_k \mathbf{P}_l = -\mathbf{P}_l \mathbf{P}_k$.

We remark that points (1), (3), (5) coincide with the defining algebraic properties of the algebra of complex numbers, quaternions, octonions, sedenions and their generalisations based on the Cayley-Dickson construction (Schafer, 2017). Therefore, the matrices in \mathcal{P} must be a representation of one of these algebras. Firstly, such algebras exist only for d that are powers of two. Secondly, matrix representations for these algebras exist only in dimension two and four. This is because the algebra of octonions and their generalisations, unlike matrix multiplication, is non-associative. As a sanity check, note that the matrices $\mathbf{R}_1, \mathbf{R}_2$ from Lemma 35 are a classic representation of the unit complex numbers.

We conclude this section by giving out the matrices for $d = 4$, which are the real matrix representations of the four unit quaternions:

$$\mathbf{R}_1 = \begin{bmatrix} 1 & 0 & 0 & 0 \\ 0 & 1 & 0 & 0 \\ 0 & 0 & 1 & 0 \\ 0 & 0 & 0 & 1 \end{bmatrix}, \quad \mathbf{R}_2 = \begin{bmatrix} 0 & -1 & 0 & 0 \\ 1 & 0 & 0 & 0 \\ 0 & 0 & 0 & -1 \\ 0 & 0 & 1 & 0 \end{bmatrix}, \quad \mathbf{R}_3 = \begin{bmatrix} 0 & 0 & -1 & 0 \\ 0 & 0 & 0 & 1 \\ 1 & 0 & 0 & 0 \\ 0 & -1 & 0 & 0 \end{bmatrix}, \quad \mathbf{R}_4 = \begin{bmatrix} 0 & 0 & 0 & -1 \\ 0 & 0 & -1 & 0 \\ 0 & 1 & 0 & 0 \\ 1 & 0 & 0 & 0 \end{bmatrix}.$$

It can be checked that these matrices respect the properties outlined above. Thus, in $d = 4$, we can select the transport maps from the set $\{\pm \mathbf{R}_1, \pm \mathbf{R}_2, \pm \mathbf{R}_3, \pm \mathbf{R}_4\}$ containing eight matrices, which also form a group. Therefore, following the same procedure as in Lemma 35, we can linearly separate up to eight classes. \square

Proposition 36. Let \mathcal{G} be the class of connected regular graphs with a finite number of classes. Then, $\mathcal{H}_{\text{orth}}^2(G)$ has linear separation power over \mathcal{G} .

Proof of Proposition 36. Idea: Since the graph is regular, the harmonic features of the nodes will be uniformly scaled and thus positioned on a circle. The aim is to place different classes at different locations on the circle, which would make the classes linearly separable as shown in Figure 4b.

Let G be a regular graph with C classes and define $\theta = \frac{2\pi}{C}$. Denote by \mathbf{R}_i the 2D rotation matrix:

$$\mathbf{R}_i = \begin{bmatrix} \cos(i\theta) & -\sin(i\theta) \\ \sin(i\theta) & \cos(i\theta) \end{bmatrix} \quad (19)$$

Then let $\mathcal{P} = \{\mathbf{R}_i \mid 0 \leq i \leq C-1, i \in \mathbb{N}\}$ the set of rotation matrices with an angle multiple of θ . Then we can define a bijection $g : \mathcal{C} \rightarrow \mathcal{P}$ and a sheaf $(G, \mathcal{F}) \in \mathcal{H}_{\text{orth}}^2(G)$ as in the proof above. Checking the inner-products from Equation 18

between the harmonic features of the nodes, we can verify that the angle between any two classes is different from zero. By Lemma 34, the cross terms of the inner product vanish:

$$\sum_k \alpha_k^2 \langle \mathbf{R}_i[k], \mathbf{R}_j[k] \rangle = \sum_k \alpha_k^2 \cos((i-j)\theta) = \cos((i-j)\theta) \|\mathbf{x}\|^2 \quad (20)$$

Thus, the angle between classes i, j is $(i-j)\theta$. \square

C. Proofs for oversmoothing

Proof of Proposition 26. Let $\mathbf{x} \in H^0(G, \mathcal{F})$. Then we have

$$\begin{aligned} 0 = E_{\mathcal{F}}(\mathbf{x}) &= \frac{1}{2} \sum_{(v,u) \in E} \|\mathcal{F}_{v \leq e} D_v^{-\frac{1}{2}} \mathbf{x}_v - \mathcal{F}_{u \leq e} D_u^{-\frac{1}{2}} \mathbf{x}_u\|^2 \\ &= \frac{1}{2} \sum_{(v,u) \in E} \|\mathcal{F}_e \left(D_v^{-\frac{1}{2}} \mathbf{x}_v - D_u^{-\frac{1}{2}} \mathbf{x}_u \right)\|^2 \\ &= \frac{1}{2} \sum_{(v,u) \in E} \|d_v^{-\frac{1}{2}} \mathbf{x}_v - d_u^{-\frac{1}{2}} \mathbf{x}_u\|^2. \end{aligned}$$

The last term vanishes if and only if $\mathbf{x}^k \in \ker \Delta_0$ for each $1 \leq k \leq d$. \square

Proposition 37. Let \mathcal{F} be an $O(d)$ -bundle over G and $\varepsilon > 0$. Assume that $\mathcal{F}_{v \leq e} = \mathcal{F}_{u \leq e}$ for each $(u, v) \neq (u_0, v_0)$ and that $\mathcal{F}_{v_0 \leq e}^\top \mathcal{F}_{u_0 \leq e} - \mathbf{I} := \mathbf{B} \neq 0$ with $\dim(\ker \mathbf{B}) > 0$. Then there exist a linear map $\mathbf{W} \in \mathbb{R}^{d \times d}$ with $\|\mathbf{W}\|_2 = \varepsilon$ and $\mathbf{x} \in H^0(G, \mathcal{F})$ such that $E_{\mathcal{F}}((\mathbf{I} \otimes \mathbf{W})\mathbf{x}) > 0$.

Proof. We sketch the proof. Let $\mathbf{g} \in \ker(\mathbf{B})$. Define then $\mathbf{x} \in C^0(G, \mathcal{F})$ by

$$\mathbf{x}_v = \sqrt{d_v} \mathbf{g}.$$

Then $\mathbf{x} \in H^0(G, \mathcal{F})$. If we now take $\mathbf{W} = \varepsilon \mathbf{P}_{\ker \mathbf{B}^\perp}$ the rescaled orthogonal projection in the orthogonal complement of the kernel of \mathbf{B} we verify the given claim. \square

We provide below a proof for the equality in Definition 24.

Proposition 38.

$$\mathbf{x}^\top \Delta_{\mathcal{F}} \mathbf{x} = \frac{1}{2} \sum_{e:=(v,u)} \|\mathcal{F}_{v \leq e} D_v^{-1/2} \mathbf{x}_v - \mathcal{F}_{u \leq e} D_u^{-1/2} \mathbf{x}_u\|_2^2$$

Proof. We prove the result for the normalised sheaf Laplacian, and other versions can be obtained as particular cases.

$$E(\mathbf{x}) = \mathbf{x}^\top \Delta_{\mathcal{F}} \mathbf{x} = \sum_v \mathbf{x}_v^\top \Delta_{vv} \mathbf{x}_v + \sum_{\substack{w \neq z \\ (w,z) \in E}} \mathbf{x}_w^\top \Delta_{wz} \mathbf{x}_z \quad (21)$$

$$= \sum_{v \leq e} \mathbf{x}_v^\top D_v^{-1/2} \mathcal{F}_{v \leq e}^\top \mathcal{F}_{v \leq e} D_v^{-1/2} \mathbf{x}_v + \sum_{\substack{w < z \\ (w,z) \in E}} \mathbf{x}_w^\top \Delta_{wz} \mathbf{x}_z + \mathbf{x}_z^\top \Delta_{zw} \mathbf{x}_w \quad (22)$$

$$= \frac{1}{2} \sum_{v, w \leq e} \left(\mathbf{x}_v^\top D_v^{-1/2} \mathcal{F}_{v \leq e}^\top \mathcal{F}_{v \leq e} D_v^{-1/2} \mathbf{x}_v + \mathbf{x}_w^\top D_w^{-1/2} \mathcal{F}_{w \leq e}^\top \mathcal{F}_{w \leq e} D_w^{-1/2} \mathbf{x}_w \right) \quad (23)$$

$$+ \mathbf{x}_v^\top D_v^{-1/2} \mathcal{F}_{v \leq e}^\top \mathcal{F}_{w \leq e} D_w^{-1/2} \mathbf{x}_w + \mathbf{x}_w^\top D_w^{-1/2} \mathcal{F}_{w \leq e}^\top \mathcal{F}_{v \leq e} D_v^{-1/2} \mathbf{x}_v \quad (24)$$

$$= \frac{1}{2} \sum_{v, w \leq e} \mathbf{x}_v^\top D_v^{-1/2} \mathcal{F}_{v \leq e}^\top (\mathcal{F}_{v \leq e} D_v^{-1/2} \mathbf{x}_v - \mathcal{F}_{w \leq e} D_w^{-1/2} \mathbf{x}_w) \quad (25)$$

$$- \mathbf{x}_w^\top D_w^{-1/2} \mathcal{F}_{w \leq e}^\top (\mathcal{F}_{v \leq e} D_v^{-1/2} \mathbf{x}_v - \mathcal{F}_{w \leq e} D_w^{-1/2} \mathbf{x}_w) \quad (26)$$

$$= \frac{1}{2} \sum_{v, w \leq e} (\mathbf{x}_v^\top D_v^{-1/2} \mathcal{F}_{v \leq e}^\top - \mathbf{x}_w^\top D_w^{-1/2} \mathcal{F}_{w \leq e}^\top) (\mathcal{F}_{v \leq e} D_v^{-1/2} \mathbf{x}_v - \mathcal{F}_{w \leq e} D_w^{-1/2} \mathbf{x}_w) \quad (27)$$

Note that D_v is symmetric for any node v and so is any $D_v^{-1/2}$. Therefore, the two vectors in the parenthesis are the transpose of each other and the result is their inner product. Thus, we have:

$$E_{\mathcal{F}}(\mathbf{x}) = \frac{1}{2} \sum_{v,w \leq e} \|\mathcal{F}_{v \leq e} D_v^{-1/2} \mathbf{x}_v - \mathcal{F}_{w \leq e} D_w^{-1/2} \mathbf{x}_w\|_2^2 \quad (28)$$

The result follows identically for other types of Laplacian. For the augmented normalized Laplacian, one should simply replace D with $\tilde{D} = D + I$ and for the non-normalised Laplacian, one should simply remove D from the equation. \square

Proof of Theorem 25. We first prove a couple of Lemmas before proving the Theorem. The structure of the proof follows that of [Cai & Wang \(2020\)](#), which in turn generalises that of [Ono & Suzuki \(2019\)](#). The latter proof technique is not directly applicable to our setting because it makes some strong assumptions about the harmonic space of the Laplacian (i.e. that the eigenvectors of the harmonic space have positive entries).

$\lambda_* = \max((\lambda_{\min} - 1)^2, (\lambda_{\max} - 1)^2)$, where $\lambda_{\min}, \lambda_{\max}$ are the smallest and largest non-zero eigenvalues of $\Delta_{\mathcal{F}}$.

Lemma 39. For $\mathbf{P} = \mathbf{I} - \Delta_{\mathcal{F}}$, $E(\mathbf{P}\mathbf{x}) < \lambda_* E_{\mathcal{F}}(\mathbf{x})$.

Proof. We can write $\mathbf{x} = \sum_i c_i \mathbf{h}^i$ as a sum of the eigenvectors $\{\mathbf{h}^i\}$ of $\Delta_{\mathcal{F}}$. Then $\mathbf{x}^\top \Delta_{\mathcal{F}} \mathbf{x} = \sum_i c_i^2 \lambda_i$, where $\{\lambda_i\}$ are the eigenvalues of $\Delta_{\mathcal{F}}$. Using this for $E_{\mathcal{F}}(\mathbf{P}\mathbf{x})$:

$$E_{\mathcal{F}}(\mathbf{P}\mathbf{x}) = \mathbf{x}^\top \mathbf{P}^\top \Delta \mathbf{P} \mathbf{x} = \mathbf{x}^\top \mathbf{P} \Delta \mathbf{P} \mathbf{x} = \sum_i c_i^2 \lambda_i (1 - \lambda_i)^2 \leq \lambda_* \sum_i c_i^2 \lambda_i = \lambda_* E_{\mathcal{F}}(\mathbf{x}) \quad (29)$$

The inequality follows from the fact that the eigenvectors of the normalised sheaf Laplacian are in the range $[0, 2]$ ([Hansen & Ghrist, 2019](#), Proposition 5.5). We note that the original proof of [Cai & Wang \(2020\)](#) bounds the expression by $(1 - \lambda_{\min})^2$ instead of λ_* , which appears to be an error. \square

Lemma 40. $E_{\mathcal{F}}(\mathbf{X}\mathbf{W}) \leq \|\mathbf{W}^\top\|_2^2 E_{\mathcal{F}}(\mathbf{X})$

Proof. Following the proof of [Cai & Wang \(2020\)](#) we have:

$$E_{\mathcal{F}}(\mathbf{X}\mathbf{W}) = \text{Tr}(\mathbf{W}^\top \mathbf{X}^\top \Delta_{\mathcal{F}} \mathbf{X} \mathbf{W}) \quad (30)$$

$$= \text{Tr}(\mathbf{X}^\top \Delta_{\mathcal{F}} \mathbf{X} \mathbf{W} \mathbf{W}^\top) \quad \text{trace cyclic property} \quad (31)$$

$$\leq \text{Tr}(\mathbf{X}^\top \Delta_{\mathcal{F}} \mathbf{X}) \|\mathbf{W} \mathbf{W}^\top\|_2 \quad \text{see Lemma 3.1 in Lee (2008)} \quad (32)$$

$$= \text{Tr}(\mathbf{X}^\top \Delta_{\mathcal{F}} \mathbf{X}) \|\mathbf{W}^\top\|_2^2 \quad (33)$$

\square

Lemma 41. For conditions as in Theorem 25, $E_{\mathcal{F}}((\mathbf{I}_n \otimes \mathbf{W})\mathbf{x}) \leq \|\mathbf{W}\|_2^2 E(f)$.

Proof. First, we note that for orthogonal matrices, $D_v = \mathbf{I} \sum_{v \leq e} \alpha_e^2 = \mathbf{I} d_v$ ([Hansen & Ghrist, 2019](#), Lemma 4.4)

$$E_{\mathcal{F}}((\mathbf{I} \otimes \mathbf{W})\mathbf{x}) = \frac{1}{2} \sum_{v,w \leq e} \|\mathcal{F}_{v \leq e} D_v^{-1/2} \mathbf{W} f_v - \mathcal{F}_{w \leq e} D_w^{-1/2} \mathbf{W} \mathbf{x}_w\|_2^2 \quad (34)$$

$$= \frac{1}{2} \sum_{v,w \leq e} \|\mathcal{F}_e \mathbf{W} (d_v^{-1/2} \mathbf{x}_v - d_w^{-1/2} \mathbf{x}_w)\|_2^2 \quad (35)$$

$$= \frac{1}{2} \sum_{v,w \leq e} \|\mathbf{W} (d_v^{-1/2} \mathbf{x}_v - d_w^{-1/2} \mathbf{x}_w)\|_2^2 \quad \mathcal{F}_e \text{ is orthogonal} \quad (36)$$

$$\leq \frac{1}{2} \sum_{v,w \leq e} \|\mathbf{W}\|_2^2 \|d_v^{-1/2} \mathbf{x}_v - d_w^{-1/2} \mathbf{x}_w\|_2^2 \quad \text{property of the operator norm} \quad (37)$$

$$= \frac{1}{2} \sum_{v,w \leq e} \|\mathbf{W}\|_2^2 \|\mathcal{F}_e (d_v^{-1/2} \mathbf{x}_v - d_w^{-1/2} \mathbf{x}_w)\|_2^2 \quad \mathcal{F}_e \text{ is orthogonal} \quad (38)$$

$$= \frac{1}{2} \|\mathbf{W}\|_2^2 \sum_{v,w \leq e} \|\mathcal{F}_e (D_v^{-1/2} \mathbf{x}_v - D_w^{-1/2} \mathbf{x}_w)\|_2^2 = \|\mathbf{W}\|_2^2 E_{\mathcal{F}}(\mathbf{x}) \quad (39)$$

The proof can also be extended easily to vector bundles over weighted graphs (i.e. allowing weighted edges as in [Ghrist & Riess \(2020\)](#)). For the non-normalised Laplacian, the assumption that \mathcal{F}_e is orthogonal can be relaxed to being non-singular and then the upper bound will also depend on the maximum conditioning number over all \mathcal{F}_e . \square

Lemma 42. *For conditions as in Theorem 25, $E_{\mathcal{F}}(\sigma(\mathbf{x})) \leq E(\mathbf{x})$.*

Proof.

$$E(\sigma(\mathbf{x})) = \frac{1}{2} \sum_{v,w \leq e} \|\mathcal{F}_{v \leq e} D_v^{-1/2} \sigma(\mathbf{x}_v) - \mathcal{F}_{w \leq e} D_w^{-1/2} \sigma(\mathbf{x}_w)\|_2^2 \quad (40)$$

$$= \frac{1}{2} \sum_{v,w \leq e} \|\mathcal{F}_e (d_v^{-1/2} \sigma(\mathbf{x}_v) - d_w^{-1/2} \sigma(\mathbf{x}_w))\|_2^2 \quad (41)$$

$$= \frac{1}{2} \sum_{v,w \leq e} \|d_v^{-1/2} \sigma(\mathbf{x}_v) - d_w^{-1/2} \sigma(\mathbf{x}_w)\|_2^2 \quad \text{orthogonality of } \mathcal{F}_e \quad (42)$$

$$= \frac{1}{2} \sum_{v,w \leq e} \|\sigma\left(\frac{\mathbf{x}_v}{\sqrt{d_v}}\right) - \sigma\left(\frac{\mathbf{x}_w}{\sqrt{d_w}}\right)\|_2^2 \quad c\text{ReLU}(x) = \text{ReLU}(cx) \text{ for } c > 0 \quad (43)$$

$$\leq \frac{1}{2} \sum_{v,w \leq e} \left\| \frac{\mathbf{x}_v}{\sqrt{d_v}} - \frac{\mathbf{x}_w}{\sqrt{d_w}} \right\|_2^2 \quad \text{Lipschitz continuity of ReLU} \quad (44)$$

$$= \frac{1}{2} \sum_{v,w \leq e} \|\mathcal{F}_e (d_v^{-1/2} \mathbf{x}_v - d_w^{-1/2} \mathbf{x}_w)\|_2^2 \quad \text{orthogonality of } \mathcal{F}_e \quad (45)$$

$$= E_{\mathcal{F}}(\mathbf{x}) \quad (46)$$

\square

Combining these three lemmas for an entire diffusion layer proves the Theorem. \square

Proof of Theorem 28. If $d = 1$, then Lemma 41 becomes superfluous as \mathbf{W}_1 becomes a scalar that can be absorbed into the right-weights. It remains to verify that a version of Lemma 42 holds in this case.

Lemma 43. *For conditions as in Theorem 28, $E_{\mathcal{F}}(\sigma(\mathbf{x})) \leq E(\mathbf{x})$.*

Proof.

$$E(\sigma(\mathbf{x})) = \frac{1}{2} \sum_{v,w \leq e} \|\mathcal{F}_{v \leq e} D_v^{-1/2} \sigma(x_v) - \mathcal{F}_{w \leq e} D_w^{-1/2} \sigma(x_w)\|_2^2 \quad (47)$$

$$= \frac{1}{2} \sum_{v,w \leq e} \|\mathcal{F}_{v \leq e} |D_v|^{-1/2} \sigma(x_v) - \mathcal{F}_{w \leq e} |D_w|^{-1/2} \sigma(x_w)\|_2^2 \quad \mathcal{F}_{v \leq e} \mathcal{F}_{w \leq e} > 0 \quad (48)$$

$$= \frac{1}{2} \sum_{v,w \leq e} \|\sigma\left(\frac{|\mathcal{F}_{v \leq e}| x_v}{\sqrt{d_v}}\right) - \sigma\left(\frac{|\mathcal{F}_{w \leq e}| x_w}{\sqrt{d_w}}\right)\|_2^2 \quad c\text{ReLU}(x) = \text{ReLU}(cx) \text{ for } c > 0 \quad (49)$$

$$\leq \frac{1}{2} \sum_{v,w \leq e} \left\| \frac{|\mathcal{F}_{v \leq e}| x_v}{\sqrt{d_v}} - \frac{|\mathcal{F}_{w \leq e}| x_w}{\sqrt{d_w}} \right\|_2^2 \quad \text{Lipschitz continuity of ReLU} \quad (50)$$

$$= \frac{1}{2} \sum_{v,w \leq e} \|\mathcal{F}_{v \leq e} D_v^{-1/2} x_v - \mathcal{F}_{w \leq e} D_w^{-1/2} x_w\|_2^2 \quad \mathcal{F}_{v \leq e} \mathcal{F}_{w \leq e} > 0 \quad (51)$$

$$= E_{\mathcal{F}}(\mathbf{x}) \quad (52)$$

□

We note that if $\mathcal{F}_{v \leq e} \mathcal{F}_{w \leq e} < 0$ (i.e. the reaction is signed), then it is very easy to find counter-examples where ReLU does not work anymore. However, the result still holds in the deep linear case. □

D. Additional model details and hyperparameters

Hybrid transport maps Consider the transport maps $-\mathcal{F}_{v \leq e}^\top \mathcal{F}_{u \leq e}$ appearing in the off the diagonal entries of the sheaf Laplacian $L_{\mathcal{F}}$. When learning a sheaf Laplacian there exists the risk that the features are not sufficiently good in the early layers (or in general) and, therefore, it might be useful to consider a hybrid transport map of the form $-\mathcal{F}_{v \leq e}^\top \mathcal{F}_{u \leq e} \oplus \mathbf{F}$, where \oplus is the direct sum of two matrices and \mathbf{F} represents a fixed (non-learnable map). In particular we consider maps of the form $-\mathcal{F}_{v \leq e}^\top \mathcal{F}_{u \leq e} \oplus \mathbf{I}_1 \oplus -\mathbf{I}_1$ which essentially appends a diagonal matrix with 1 and -1 on the diagonal to the learned matrix. From a signal processing perspective, these correspond to a low-pass and a high-pass filter that could produce generally useful features. We treat the addition of these fixed parts as an additional hyper-parameter.

Adjusting the activation magnitudes We note that in practice we find it useful to learn an additional parameter $\varepsilon \in [-1, 1]^d$ (i.e. a vector of size d) in the discrete version of the models:

$$\mathbf{X}_{t+1} = (1 + \varepsilon) \mathbf{X}_t - \sigma\left(\Delta_{\mathcal{F}(t)}(\mathbf{I} \otimes \mathbf{W}_1^t) \mathbf{X}_t \mathbf{W}_2^t\right). \quad (53)$$

This allows the model to adjust the relative magnitude of the features in each stalk dimension. This is used across all of our experiments in the discrete models.

Augmented normalised sheaf Laplacian Similarly to GCN which normalises the Laplacian by the augmented degrees (i.e. $(\mathbf{D} + \mathbf{I}_n)^{-1/2}$, where \mathbf{D} is the usual diagonal matrix of node degrees), we similarly use $(D + \mathbf{I}_{nd})^{-1/2}$ for normalisation to obtain greater numerical stability. This is particularly helpful when learning general sheaves as it increases the numerical stability of SVD.

Learning sheaves and the k -WL test According to our theoretical results, one should learn a pair of non-equal restriction maps along the edges between two classes. Suppose this is done via a local functions $\mathcal{F}_{v \leq e := (v,u)} = \phi(\mathbf{x}_v, \mathbf{x}_u)$. Then, $\phi(\mathbf{x}_v, \mathbf{x}_u) \neq \phi(\mathbf{x}_u, \mathbf{x}_v)$ only if $\mathbf{x}_u \neq \mathbf{x}_v$. This leads to the following remark.

Remark. Let G be a graph with an initial colouring \mathbf{x} such that $\exists (v,u) \in E$ and v and u are not k -WL distinguishable. Then no model upper bounded by k -WL can learn an asymmetric relation along the edge (v,u) .

This observation motivates our decision to evolve the geometry at each layer of the model since at initialisation time many nodes might not be distinguishable. At the same time, it suggests that provably expressive architectures might be able to learn better sheaves (see ablation study in Appendix E).

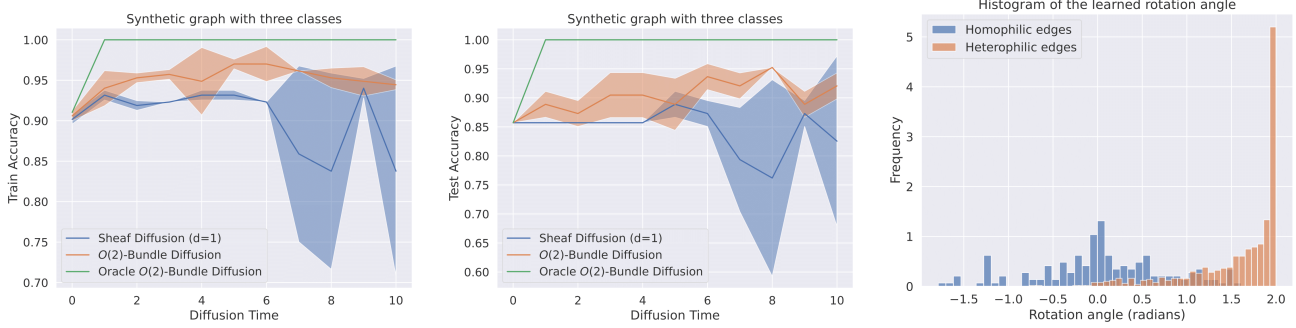


Figure 5. (Left) Train accuracy as a function of diffusion time. (Middle) Test accuracy as a function of diffusion time. (Right) Histogram of the learned rotation angle of the 2D transport maps. The performance of the bundle model is superior to that of the one-dimensional sheaf. The transport maps learned by the model are aligned with our expectation: the model learns to rotate more (i.e. to move away) the neighbours belonging to different classes than the neighbours belonging to the same class.

Hyperparameters for discrete models For the discrete models we searched in the following hyperparameters:

- Hidden channels: [8, 16, 32] for WebKB datasets and [8, 16, 32, 64] for all the other datasets.
- d : [1, 2, 3, 4, 5]
- Layers: [2, 3, 4, 5, 6, 7, 8]
- Learning rate: 0.02 for the WebKB datasets and 0.01 for all the other datasets.
- Weight decay for the regular model parameters: searched in a log-uniform range over $[-4.5, 11.0]$
- Weight decay for the parameters learning the sheaf: searched in a log-uniform range over $[-4.5, 11.0]$
- Dropout on the inputs: searched uniformly over $[0, 0.9]$.
- Dropout for the other layers: searched uniformly over $[0, 0.9]$.
- Early stopping patience: 100 epochs for the Wiki datasets and 200 for the others.
- Maximum training epochs: 1000 epochs for the Wiki datasets and 500 for the others.

Hyperparameters for continuous models For the continuous models we searched over the following hyperparameters:

- Hidden channels: [8, 16, 32, 64]
- d : [1, 2, 3, 4, 5]
- Learning rate: searched in a log-uniform range over $[0.01, 0.1]$
- Weight decay: searched in a log-uniform range over $[-6.9, 13.8]$
- Dropout: searched uniformly in $[0, 0.95]$.
- ODE Integration method: euler.
- Maximum integration time: searched uniformly over $[1.0, 9.0]$.
- Training epochs: 50.

We train all models using the Adam optimiser (Kingma & Ba, 2015). All models use ELU activations.

E. Additional Experiments

In this section we provide a series of additional experiments and ablation studies.

Two dimensional synthetic experiment In the main text we focused on a synthetic example involving sheaves with one-dimensional stalks. We now consider a graph with three classes and two-dimensional features, with edge homophily level 0.2. We use 80% of the nodes for training and 20% for testing. First, we know that a discrete vector bundle with two-dimensional stalks that can solve the task in the limit exists from Theorem 23, while based on Proposition 19 no sheaf with one-dimensional stalks can perfectly solve the tasks.

	Eigenvectors	Texas	Wisconsin	Cornell
Cont Diag-SD	0	82.97 \pm 4.37	86.47 \pm 2.55	80.00 \pm 6.07
	2	3.51 \pm 5.05	85.69 \pm 3.73	81.62 \pm 8.00
	8	85.41 \pm 5.82	86.28 \pm 3.40	82.16 \pm 5.57
	16	82.70 \pm 3.86	85.88 \pm 2.75	81.08 \pm 7.25
Cont $O(d)$ -SD	0	82.43 \pm 5.95	84.50 \pm 4.34	72.16 \pm 10.40
	2	84.05 \pm 5.85	85.88 \pm 4.62	83.51 \pm 9.70
	8	84.87 \pm 4.71	86.86 \pm 3.83	84.05 \pm 5.85
	16	83.78 \pm 6.16	85.88 \pm 2.88	83.51 \pm 6.22
Cont Gen-SD	0	83.78 \pm 6.62	85.29 \pm 3.31	84.60 \pm 4.69
	2	83.24 \pm 4.32	84.12 \pm 3.97	81.08 \pm 7.35
	8	82.70 \pm 5.70	84.71 \pm 3.80	83.24 \pm 6.82
	16	82.16 \pm 6.19	86.47 \pm 3.09	82.16 \pm 6.07

Table 2. Ablation study for the dimension of the stalks. Positional encodings improve performance on some of our models.

Therefore, similarly to the synthetic experiment in the main text, we compare two similar models learning the sheaf from data: one using 1D stalks and another using 2D stalks. As we see from Figure 5, the discrete vector bundle model has better training and test-time performance than the one-dimensional counterpart. Nonetheless, none of the two models manages to match the perfect performance of the ideal sheaf on this more challenging dataset. From the final subfigure we also see that the model learns to rotate more across the heterophilic edges in order to push away the nodes belonging to other classes. The prevalent angle of this rotation is 2 radians, which is just under $120^\circ = 360^\circ/C$, where $C = 3$ is the number of classes. Thus the model learns to position the three classes at approximately equal arc-lengths from each other for maximum linear separability.

Positional encoding ablation Based on the Remark from the previous section, we proceed to analyse the impact of increasing the expressive power of the model by making the nodes more distinguishable. For that, we equip our datasets with additional features consisting of graph Laplacian positional encodings as originally done in Dwivedi et al. (2020). In Table 2 we see that positional encodings do indeed improve the performance of the continuous models compared to the numbers reported in the main table. Therefore, we conclude that the interaction between the problem of sheaf learning and that of the expressivity of graph neural networks represents a promising avenue of future research.

Visualising diffusion To develop a better intuition of the limiting behaviour of sheaf diffusion for node classification tasks we plot the diffusion process using an oracle discrete vector bundle for two graph with $C = 3$ (Figure 7) and $C = 4$ (Figure 6) classes. The diffusion processes converges in the limit to a configuration where the classes are rotated at $\frac{2\pi}{C}$ from each other, just like in the cartoon diagrams of Figure 4. Note that in all cases, the classes are linearly separable in the limit.

We note that this approach generalises to any number of classes, but beyond $C = 4$ it is not guaranteed that they will be linearly separable in 2D. However, they are still well-separated. We include an example with $C = 10$ classes in Figure 8.

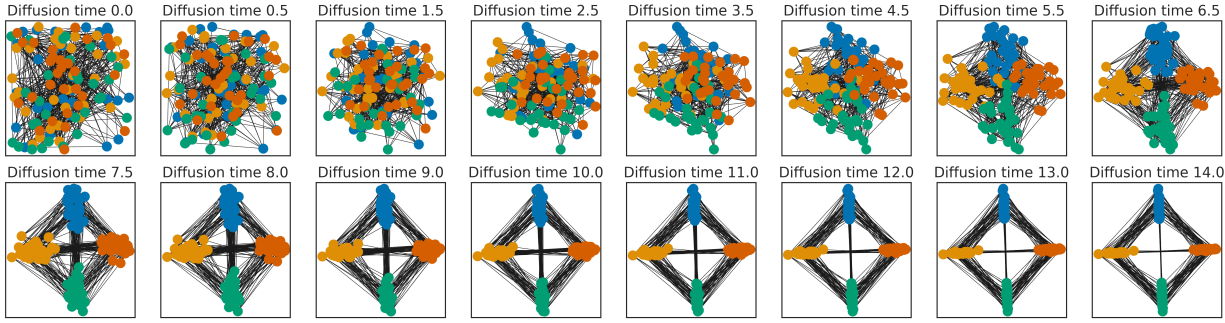


Figure 6. Sheaf diffusion process disentangling the $C = 4$ classes over time. The nodes are coloured by their class.

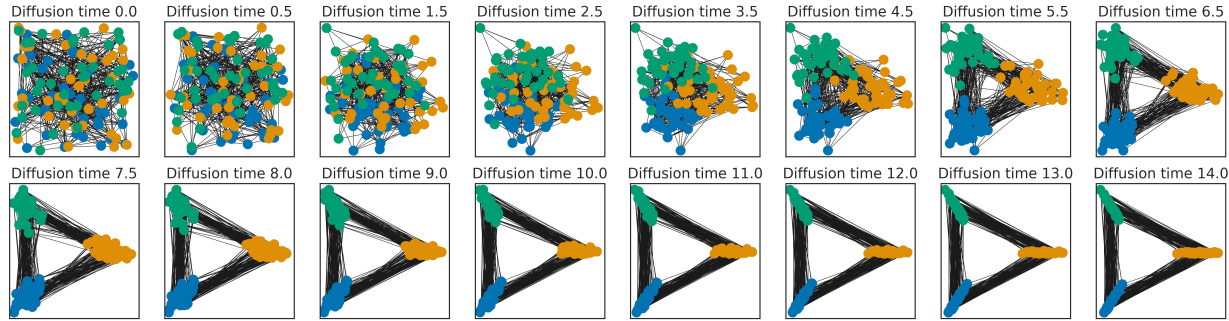


Figure 7. Sheaf diffusion process disentangling the $C = 3$ classes over time. The nodes are coloured by their class.

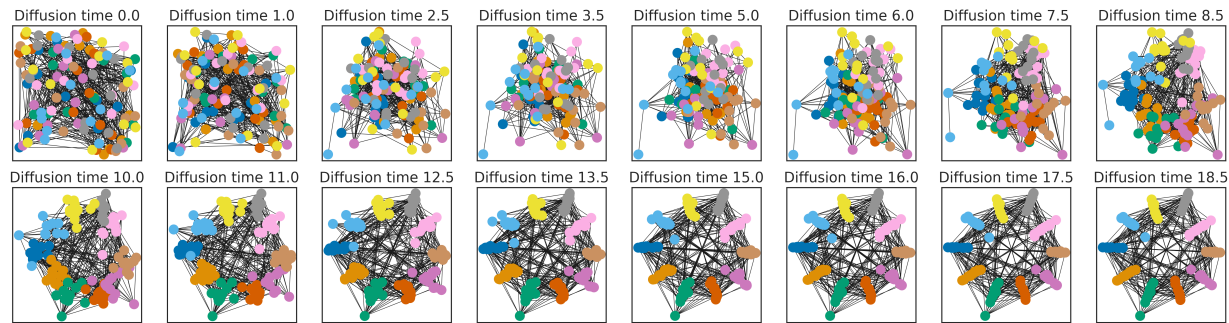


Figure 8. Sheaf diffusion process disentangling the $C = 10$ classes over time. The nodes are coloured by their class.